JOURNAL OF PETROLOGY | VOLUME 46 | NUMBER 2 | PAGES 221–253 | 2005 | doi:10.1093/petrology/egh065

Cenozoic Magmatism of the North-Eastern Eurasian Margin: The Role of Lithosphere Versus Asthenosphere

SATOSHI OKAMURA[1]*, RICHARD J. ARCULUS[2] AND YURI A. MARTYNOV[3]

[1]SAPPORO CAMPUS, HOKKAIDO EDUCATION UNIVERSITY, SAPPORO 002-8502, JAPAN

[2]DEPARTMENT OF EARTH AND MARINE SCIENCES, AUSTRALIAN NATIONAL UNIVERSITY, CANBERRA, ACT 0200, AUSTRALIA

[3]FAR EAST GEOLOGICAL INSTITUTE, VLADIVOSTOK 690022, RUSSIA

RECEIVED MAY 12, 2003; ACCEPTED JULY 26, 2004
ADVANCE ACCESS PUBLICATION OCTOBER 14, 2004

Sikhote-Alin and Sakhalin are located in the Russian Far East flank of the northernmost part of the Sea of Japan. Magmatism in this region preceded, was concurrent with, and continued after the extension and sea-floor spreading (25–18 Ma) that formed the Sea of Japan. Among the Sikhote-Alin and Sakhalin volcanic suites, Eocene–Oligocene (55–24 Ma) lavas are characterized by greater large ion lithophile element and rare earth element enrichments compared with Early–Mid-Miocene (23–15 Ma) tholeiites, and also show a depletion in high field strength elements (HFSE). The geochemical characteristics of the Eocene–Oligocene and Early–Mid-Miocene basalts are consistent with migration of the locus of magma generation beneath the Sikhote-Alin and Sakhalin areas from subduction-modified lithospheric mantle into mid-ocean ridge basalt (MORB)-source asthenosphere as spreading in the Sea of Japan progressed. Mid-Miocene–Pliocene (14–5 Ma) lavas, erupted following the opening of the Sea of Japan, include alkaline and sub-alkaline basalts with wide ranges in trace element abundances, varying between two distinct end-members: (1) volumetrically minor alkaline basalts with Zr–Nb and Sr–Nd–Pb isotope compositions similar to asthenosphere-derived, intra-plate–hot-spot basalts from eastern China; (2) more abundant, lithosphere-derived, low-alkali tholeiites depleted in HFSE. The similarity of isotopic signatures coupled with systematically different rare earth element (REE) abundances in the Mid-Miocene–Pliocene and Chinese basalts are best modeled by similar extents of melting of spinel lherzolite and garnet lherzolite, respectively. The Mid-Miocene–Pliocene alkali basalts were generated by small degrees of partial melting of hot asthenosphere beneath a thin lithospheric lid; the thin lithospheric mantle beneath the Sikhote-Alin and Sakhalin region resulted from heating and extension associated with the opening of the Sea of Japan.

KEY WORDS: *north-eastern Eurasian margin; Sikhote-Alin–Sakhalin; Japan Sea opening; subcontinental lithosphere; asthenosphere*

INTRODUCTION

The north-eastern margin of the Eurasian continent in the area of coastal Sikhote-Alin and Sakhalin has been affected by subduction since the Mesozoic (Zonenshain *et al.*, 1990), and by extension during formation of the Sea of Japan in the Cenozoic (Tamaki *et al.*, 1992; Jolivet *et al.*, 1995) (Fig. 1). This region provides an important opportunity to study temporal changes in magma source regions accompanying the evolution of subduction- and extension-related magmatic provinces, and specifically during the opening of a back-arc basin (Sea of Japan). Until recently, little was known about the chemical composition of the Cenozoic volcanic rocks from Sikhote-Alin and Sakhalin, although previous studies suggested that there was a change from subduction-related to intra-plate-type magmatism as the Sea of Japan opening progressed (Esin *et al.*, 1995; Okamura *et al.*, 1998*a*; Tatsumi *et al.*, 2000). Petrological and geochemical studies of these rocks have been used to evaluate the changing nature of the mantle source regions of the magmatism associated

*Corresponding author. Telephone/fax: 81 11 778 0386. E-mail: okamura@sap.hokkyodai.ac.jp

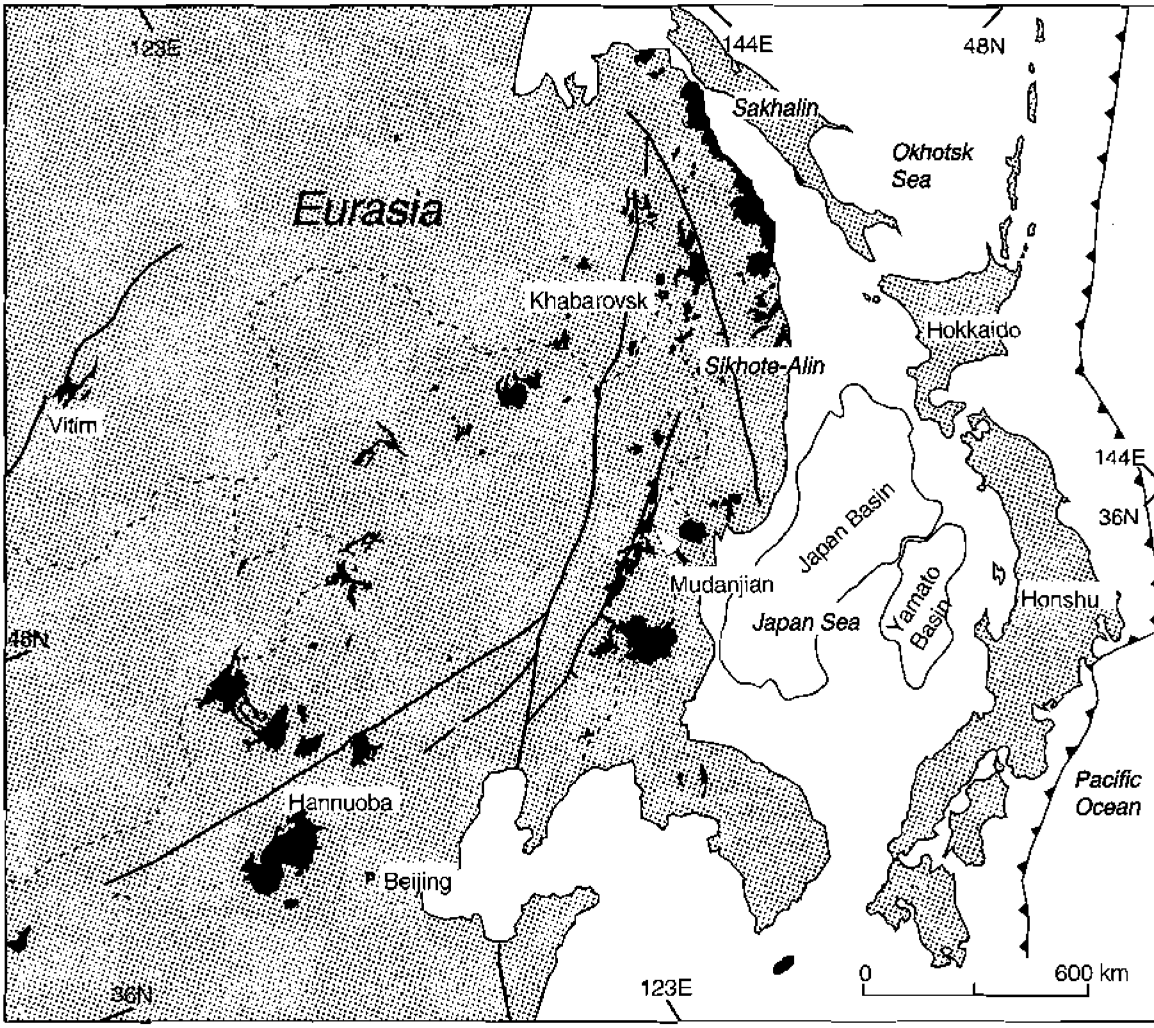

Fig. 1. Map of the north-eastern Eurasian margin showing the location of major Cenozoic volcanic fields in black. Major faults are indicated by black lines, with the deep-sea trench marking the present site of subduction of the Pacific Plate decorated with solid triangles.

with this active continental margin. Based on a detailed Sr–Nd–Pb isotope study, Okamura *et al.* (1998*a*) identified temporal geochemical trends in the Sikhote-Alin and Sakhalin volcanic rocks that suggest that asthenospheric mantle flow from beneath north-east China, which resulted in the formation of intra-plate-type basalts, triggered the opening of the Sea of Japan. Conversely, Tatsumi *et al.* (2000) interpreted variations in the K/Y and K/Nb ratios of Sikhote-Alin basalts to indicate that subduction-related magmatism was terminated by opening of the Sea of Japan, and that intraplate-type magmas were subsequently produced. To gain a better understanding of the relationship of changing magma sources to the opening of back-arc basins, we have obtained a more comprehensive major- and trace-element and Sr–Nd–Pb isotope dataset for the lavas of our previous study (Okamura *et al.*, 1998*a*). These new data are used to identify the most primitive magmas, evaluate the role of crustal contamination, constrain the nature of the mantle source regions, and develop models for magma generation processes. Comparisons are made between the chemical and isotopic composition of these lavas and those of north-east China, including the Middle Miocene–Pliocene Hannuoba basalts (Zhi *et al.*, 1990; Fan & Hooper, 1991) and the Late Miocene–Holocene Mudanjian basalts (Fan & Hooper, 1991) shown in Fig. 1. These data provide important constraints on the tectonic evolution of the Eurasian continental margin, and the relationship between extension- and subduction-related magmatism during opening of the Sea of Japan.

GEOLOGICAL SETTING

Upper Cretaceous to Pliocene volcanic–plutonic rocks are widely distributed along the north-eastern Eurasian continental margin. The Mesozoic volcanic–plutonic

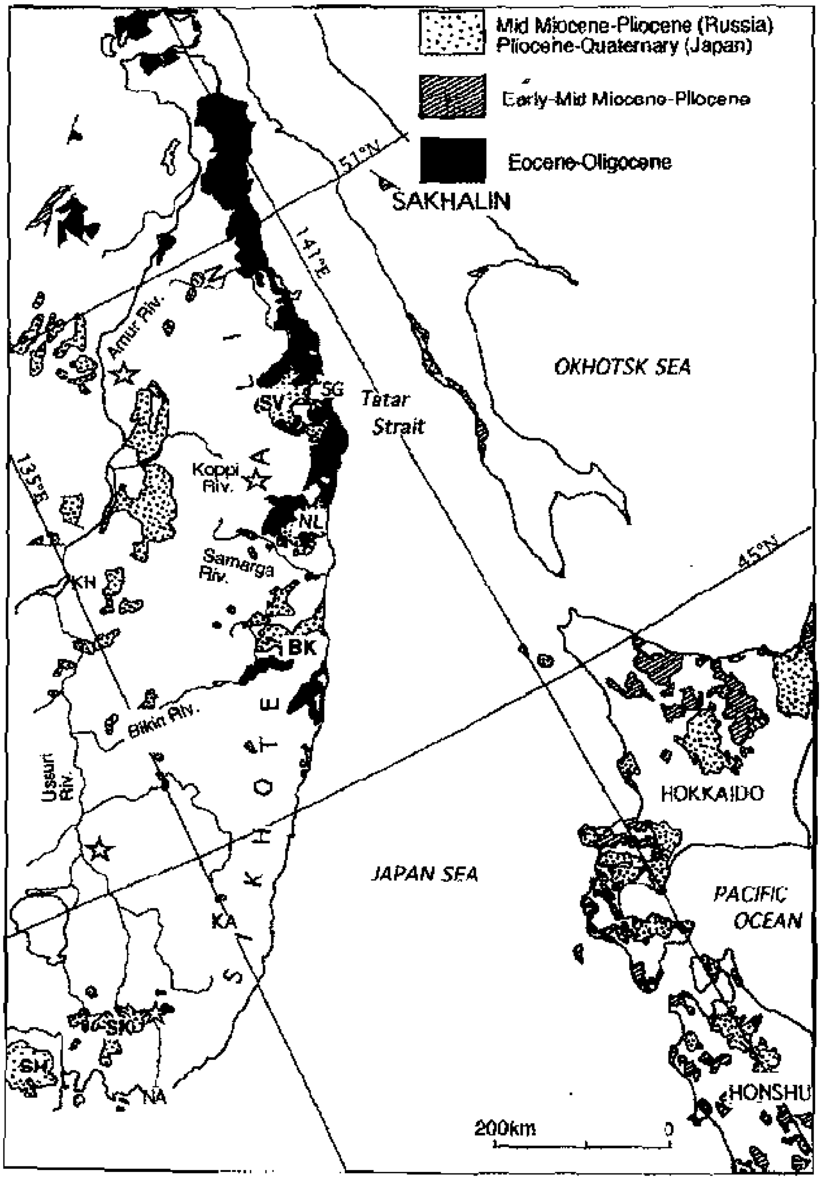

Fig. 2. *Map of the Sikhote-Alin- Sakhalin* and northern Japan region. Ultramafic xenolith occurrences are indicated by open stars (Ionov *et al.*, 1995). Abbreviations for volcanic fields in Sikhote-Alin–Sakhalin: SV, Sovgavan Plateau; NL, Nelma Plateau; BK, Bikin Plateau; SK, Shkotovo Plateau; SH, Shufan Plateau; SG, Sovgavan; KH, Khabarovsk; KA, Kavalerovo; NA, Nakhodka.

belts developed in an Andean-type tectonic setting related to subduction of the Izanagi Plate (Zonenshain *et al.*, 1990). Subsequently, basaltic volcanism occurred along the Sea of Japan coast to the Tatar Strait during the Eocene to Early Pliocene (Fig. 2). Changes in the compositions of the Cenozoic basaltic rocks reflect a change over 55 Myr from a supra-subduction zone- to a continental rift tectonic setting, as the Sea of Japan opened between eastern Sikhote-Alin and the islands forming Japan. Paleomagnetic studies indicate that sea-floor spreading has resulted in eastward migration of the Japan arc away from eastern Sikhote-Alin, producing the Japan and Yamato Basins (Otofuji & Matsuda, 1984; Otofuji *et al.*, 1994). Ar–Ar ages of seafloor basalts as well as the magnetic anomaly pattern in the Japan Basin indicate that sea-floor spreading occurred from about 28 to 18–Ma (Tamaki *et al.*, 1992).

Based on field data, together with 30 K–Ar dates (Okamura *et al.*, 1998*b*), the volcanism of the Sikhote-Alin and Sakhalin region comprises three distinct stages: (1) subduction-related, active continental-margin volcanism in the Eocene–Oligocene (55–24 Ma) along the north-eastern edge of Eurasia, pre-dating and concurrent with the opening of the Sea of Japan, and contemporaneous with the eruption of extension-related, within-plate basalts associated with north-east-trending grabens in north-east China; (2) Early–Mid-Miocene (23–15 Ma) subduction-related volcanism surrounding the opening Sea of Japan in Sikhote-Alin–Sakhalin and the frontal Japanese island arc; relatively few samples from central Sikhote-Alin and Sakhalin have yielded dates in this period; (3) Mid-Miocene–Pliocene (14–5 Ma) volcanism in Sikhote-Alin and Sakhalin, post-dating the opening of the Sea of Japan, forming plateau basalts filling interfluves. The Mid-Miocene–Pliocene lavas occur along the Sea of Japan coast up to the Tatar Strait in central and south Sikhote-Alin, comprising five plateaux from north to south: Sovgavan, Nelma and Bikin in central Sikhote-Alin, and Shukotovo and Shufan in south Sikhote-Alin (Fig. 2). The Mid-Miocene–Pliocene basaltic sequences are characterized by a large number of fissure-fed lava flows, locally totalling ~200 m thicknesses.

SAMPLES AND PETROGRAPHY

Cenozoic Sikhote-Alin and Sakhalin volcanic rocks include alkali olivine basalts, olivine basalts and basaltic andesites. CIPW norms indicate that compositions range from tholeiite (qz- and ol-normative) to alkali basalt (normative ne $\leq$ 5%) and basanite (ne $>$ 5%) (Fig. 3). For simplicity, basanites are included with alkali basalts in the following discussion. The Early–Mid-Miocene lavas are ol- to qz-normative tholeiites, whereas the Eocene–Oligocene and Mid-Miocene–Pliocene lavas span a broad range from ne- to qz-normative compositions. More than 70% of the Middle Miocene–Pliocene basalts are qz- and ol-normative, with the remainder mildly to moderately ne-normative. The Sovgavan Plateau has a great thickness of qz- and ol-normative tholeiite flows (>230 m), with alkali basalts in lesser amounts mostly in the upper levels. The Nelma, Shukotovo and Shufan Plateaux are composed predominantly of quartz and olivine tholeiite flows, inter-layered with small amounts of alkali basalt (<1–5%) (Okamura *et al.*, 1998*b*). The Late Miocene–Holocene Mudanjian basalts consist of ne-normative ($\geq$5%) alkali basalts and basanites.

Point-counted phenocryst modes are listed in Table 1 for 48 representative samples. The Sikhote-Alin and Sakhalin volcanic rocks are mostly sparsely phyric, with a primary mineral assemblage of plagioclase, olivine, clinopyroxene, titanomagnetite and ilmenite. The average volume percentage of primary phenocrysts and microphenocrysts approaches 50% in the Early–Mid-Miocene units, but is much lower in the Mid-Miocene–Pliocene and Eocene–Oligocene rocks. The Eocene–Oligocene basalts typically have $\leq$10% olivine (Fo_{77-84}) and plagioclase (An_{64-78} Ab_{21-34} Or_1) phenocrysts. Olivine phenocrysts commonly contain Cr–Al Mg-rich spinel inclusions (Cr_2O_3 ~ 27%, Al_2O_3 ~ 23%). The Early–Mid-Miocene basalts are markedly porphyritic with 20–51% olivine (Fo_{68-90}), clinopyroxene (En_{39-46} Fs_{10-15} Wo_{42-48}) and plagioclase (A_{77-95} Ab_{5-23} $Or_{0.2-1}$), with small amounts of orthopyroxene and titanomagnetite. Olivine, clinopyroxene and plagioclase phenocrysts commonly contain spinel inclusions with ~13% Cr_2O_3 and ~24% Al_2O_3. The olivine and quartz tholeiites that dominate among the Mid-Miocene–Pliocene basalts typically have 10–16% phenocrysts of mostly olivine (Fo_{76-84}) and plagioclase (An_{10-53} Ab_{45-70} Or_{1-31}), with small amounts of clinopyroxene (En_{36-43} Fs_{12-14} Wo_{43-48}). Olivine phenocrysts commonly contain Cr–Al- Mg-rich spinel inclusions (Cr_2O_3 ~ 25%, Al_2O_3 ~ 30%). The alkali basalts and basanites typically have <16% olivine (Fo_{77-79}), clinopyroxene (En_{39-48} Fs_{10-13} Wo_{42-48}) and plagioclase (An_{47-51} Ab_{43-47} Or_{2-4}). Mid-Miocene–Pliocene basalts commonly contain mantle xenoliths of spinel lherzolite and websterite, orthopyroxenites of unknown provenance, and megacrysts of olivine, clinopyroxene and orthopyroxene. The Late Miocene–Holocene Mudanjian basalts are sparsely phyric with 1–8% olivine and clinopyroxene phenocrysts.

GEOCHEMISTRY

Analytical methods

Major and trace element data for 41 rocks from Sikhote-Alin, Sakhalin and Mudanjian from north-east China (Fig. 1) ~800 km SW of Sikhote-Alin and Sakhalin are reported in Table 2. A total of 93 samples have been analyzed, and all of these data are utilized in the figures. The complete dataset is included in Electronic Appendix A. Major element concentrations were analysed by X-ray fluorescence (XRF) using fused discs either at Hokkaido University or the Smithsonian Institution. Trace element concentrations were measured by XRF using pressed powder pellets at the Smithsonian Institution, and by inductively coupled plasma-mass spectroscopy (ICP–MS) at the Macquarie University Geochemical Analysis Unit and the Geoanalytical Laboratory of Washington State University. Rb, Sr, Sm and Nd concentrations in five samples were determined by isotope dilution (ID) at Okayama University (Table 3). Precisions (reproducibilities, standard deviation 1σ/mean) for XRF are <1% for major elements, and around 5% for trace elements. Precisions for all ICP–MS and ID elements are <3%, except for Th and U at 9%.

Strontium and neodymium isotope analyses were determined for 38 samples; 17 of these were also analysed for lead isotopes (Table 3). Pb-isotope analyses were performed by thermal ionization mass spectrometery at the University of California, Los Angeles (UCLA)

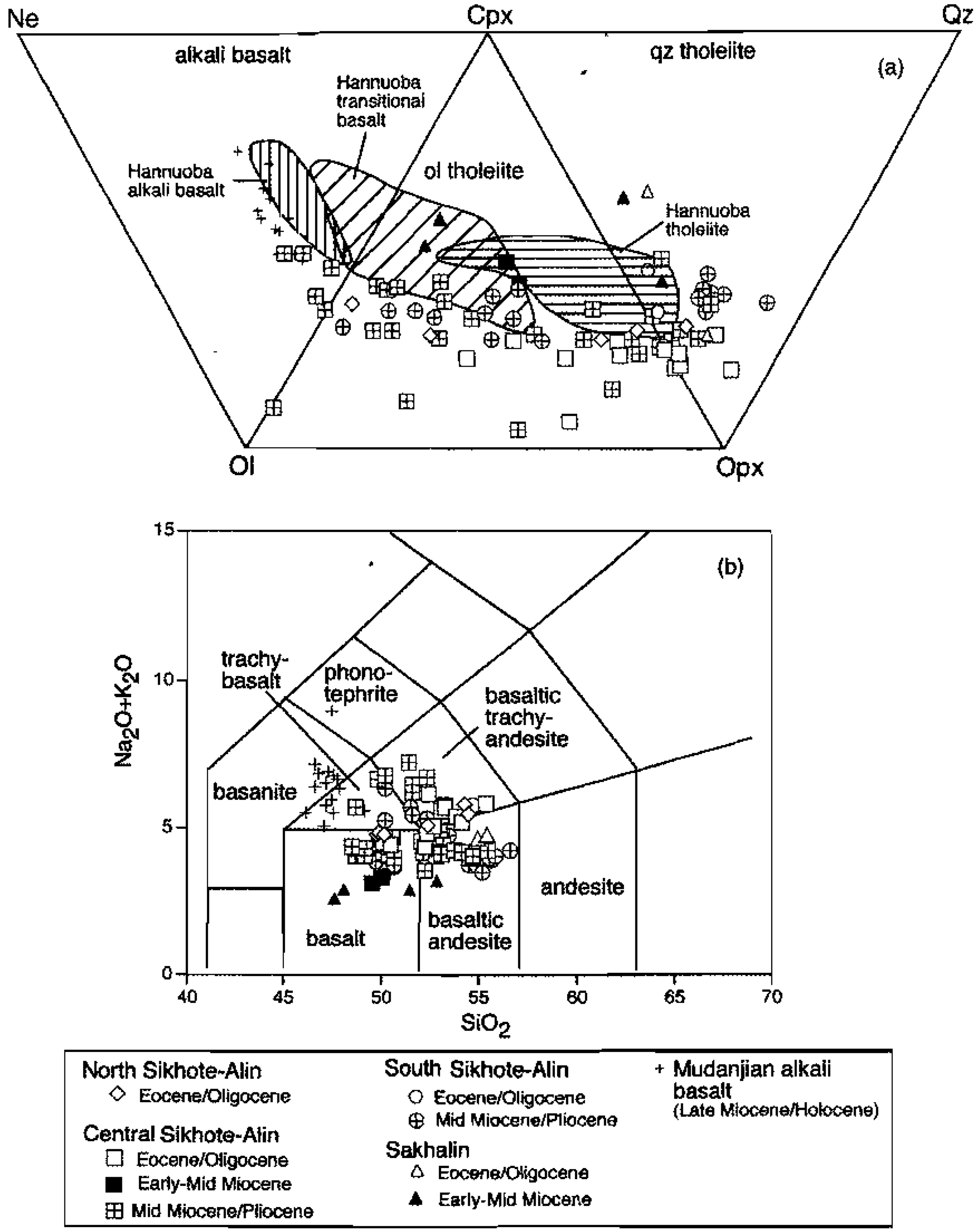

Fig. 3. (a) Classification diagram for volcanic rocks of the Sikhote-Alin–Sakhalin and Mudanjian area based on their CIPW normative compositions projected in Ne–Ol–Cpx–Opx–Qz compositional space after Thompson (1984); (b) total alkali vs wt % SiO_2 for volcanic rocks of the Sikhote-Alin Sakhalin and Mudanjian area. Fields after Le Maitre *et al.* (2002).

using a VG 7-collector Sector 54 thermal source mass spectrometer. Sr and Nd isotope measurements were performed at Okayama University. Mass spectrometric analyses were made following the procedure of Kagami *et al.* (1987, 1989). The Pb-isotope analyses are normalized to US National Bureau of Standards standard 981 (NBS981) values. Reproducibilities for Pb are $\leq 0{\cdot}05\%$ per a.m.u. Blanks for Pb are <500 pg, and are

Table 1: Point-counted phenocryst modes (vol. %) for representative volcanic rocks of Sikhote-Alin–Sakhalin and Mudanjian (>1000 points for each sample)

	Opq	Bio	Opx	Pl	Cpx	Ol	Gm	Total
Mid-Miocene—Pliocene								
(alkali basalt)								
YuS21/B						9·4	90·6	100·0
YuM1381				0·6	0·8	3·1	95·5	100·0
YuM1328				0·8	1·1	2·2	95·9	100·0
(olivine tholeiite)								
Yu84	1·1	0·4		10·5	1·4	1·3	85·2	100·0
YuS108/10				0·2			99·8	100·0
P369/13				5·0		4·2	90·8	100·0
Yu68				16·2	0·8	1·1	81·9	100·0
SO-36						3·0	97·0	100·0
YuM1787						2·7	97·3	100·0
YuS108/4						8·9	91·1	100·0
ALKB					0·3	5·6	94·1	100·0
YuS108/6						6·5	93·5	100·0
Yu85	1·4	0·8		9·3	2·5	1·6	84·3	100·0
YuS979						3·2	96·8	100·0
P369/11				0·4		7·6	92·0	100·0
P369/11b				2·4		5·2	92·4	100·0
(quartz tholeiite)								
SO-73				0·8		6·3	92·9	100·0
SO-29							100·0	100·0
YuM1120				0·1		1·2	98·8	100·0
YuS120/9							100·0	100·0
VS-3			2·3	4·3			93·4	100·0
P369/2							100·0	100·0
VS-1							100·0	100·0
Early-Mid-Miocene								
Yu17				12·9	3·8	3·8	79·5	100·0
Yu19				20·4	9·2	9·7	60·8	100·0
S-3	0·1		1·8	22·7			75·5	100·0
S-11	1·2			34·1	8·2	7·1	49·4	100·0
SA-02	0·6			27·4	8·5	9·7	53·8	100·0
SA-04	0·8		1·5	25·8	3·6	7·1	61·2	100·0
Eocene—Oligocene								
(olivine tholeiite)								
SO-13				0·4			99·6	100·0
YuM609				2·9		2·8	94·3	100·0
Yu770				3·4		6·5	90·0	100·0
YuM537				0·7		2·2	97·1	100·0
YuS122/7				4·7		3·4	91·9	100·0
Yu155/1B				2·0		2·4	95·6	100·0
YuS122/13				4·7		4·9	90·4	100·0
YuS122/14						3·1	96·9	100·0
Yu7				0·6		4·5	94·9	100·0
SO-17					0·5	0·5	99·0	100·0

	Cpq	Bio	Opx	Pl	Cpx	Ol	Gm	Total
(quartz tholeiite)								
SO-9						0·6	99·4	100·0
K-01				1·2		3·6	95·2	100·0
SO-23						3·5	96·5	100·0
SO-62				1·5		2·1	96·4	100·0
YuS122/8						3·1	96·9	100·0
S-12A				2·1		2·0	95·9	100·0
YuM1119				2·0		4·5	93·5	100·0
S-17				8·2	0·7	7·3	83·8	100·0
Mudanjian								
J-8						7·8	92·2	100·0

Opq, opaque minerals; Bio, biotite; Opx, orthopyroxene; Pl, plagioclase; Cpx, clinopyroxene; Ol, olivine; Gm, groundmass. Phenocrysts are defined as more than 0·03 mm in size, consisting of phenocryst (>0·3 mm) and microphenocryst (0·03–0·3 mm) following Wilcox (1954).

negligible for these analyses. The $^{87}Sr/^{86}Sr$ and $^{143}Nd/^{144}Nd$ ratios are normalized to $^{86}Sr/^{88}Sr$ = 8·375209 and $^{146}Nd/^{144}Nd$ = 0·7219, respectively. The measured $^{87}Sr/^{86}Sr$ ratio for NBS987 during this study is 0·710248 ± 0·000008 ($N = 3$). Mean analytical uncertainty for sample during this study is ±0·00002 (2σ). The $^{143}Nd/^{144}Nd$ ratios are reported relative to $^{143}Nd/^{144}Nd$ = 0·512640 for BCR-1 (Wasserburg *et al.*, 1981). Mean analytical uncertainty for sample during this study is ±0·00002 (2σ).

Major-element compositions

All of the studied samples have <56·5 wt % SiO_2. Major element oxides for the Sikhote-Alin and Sakhalin lavas are plotted vs MgO as an index of differentiation in Fig. 4. A distinctive compositional feature of the basalts is broad scatter in K_2O, Na_2O, FeO, TiO_2 and P_2O_5 contents of both the Mid-Miocene–Pliocene and the Eocene–Oligocene groups. The overall variations probably result from variable fractional crystallization effects superimposed on a range of parent melts. The Early–Mid-Miocene basalts comprise quartz and olivine tholeiites, characterized by higher CaO and lower TiO_2, Na_2O and P_2O_5 than any other Sikhote-Alin and Sakhalin basalts at equivalent MgO contents. They fall into the tholeiitic field on the SiO_2 vs FeO^*/MgO discriminant diagram (Miyashiro, 1974), and have composition typical of island-arc tholeiites. TiO_2 contents are consistently lower in all the Early–Mid-Miocene basalts, and the Eocene–Oligocene basalts from Sakhalin, most of which contain <1 wt % TiO_2 compared with >1 wt % for all the Mid-Miocene–Pliocene basalts and the Eocene–Oligocene basalts from Sikhote-Alin.

Trace-element compositions

Among the Sikhote-Alin and Sakhalin volcanic rocks, a subset of the Early–Mid-Miocene tholeiites is distinctive on the basis of markedly low high field strength element (HFSE) abundances. The greatest depletion occurs at Nb and Ta on MORB-normalized trace-element variation diagrams (Fig. 5c), similar to depletions that are commonly observed in island-arc volcanic rocks (Gill, 1981). The Eocene–Oligocene lavas are characterized by both large ion lithophile element (LILE) and REE enrichments compared with the depleted Early–Mid-Miocene tholeiites, but also show a relative depletion in HFSE, even though Nb and Ta show only a weak negative anomaly compared with the adjacent elements (Fig. 5d). The enriched Eocene–Oligocene basalts closely resemble active-continental-margin basalts which have an enriched subcontinental lithospheric mantle component in their source (Pearce, 1983). Relatively high abundances of K, Ba and Pb are additional features of both the Early–Mid-Miocene and the Eocene–Oligocene rocks. The Mid-Miocene–Pliocene lavas from all the plateaux exhibit wide ranges in trace-element abundances and patterns that vary between two distinct end-member types. At one extreme, alkali basalts have fairly smooth MORB-normalized patterns (Fig. 5a). These patterns are nearly indistinguishable from those of intra-plate, ocean island alkali basalts (OIB; e.g. Sun & McDonough, 1989), consistent with their derivation from an asthenospheric mantle source, without significant contamination by lithospheric mantle or crustal material. In contrast, quartz and olivine tholeiites form the other extreme, exhibiting only slight light REE (LREE) enrichment, low LILE abundances, but high abundances of Ba, Pb and Sr. Some of the quartz tholeiites from south

Table 2: Major- and trace-element analyses of representative volcanic rocks of Sikhote-Alin-Sakhalin and Mudanjian by XRF and ICP-MS

	Mid-Miocene—Pliocene (14–5 Ma)							
Sample no.:	YuM1381[1]	YuM1328[2]	Yu84[2]	YuS108/10[1]	P369/13[2]	SO-36[2]	YuM1787[2]	YuS108/6[1]
Age (Ma):[3]	9·9	11·9			8·7	5·0	5·4	8·1
Locality:	Koppi riv.	Koppi riv.	Sovgavan Pl	Sovgavan Pl	Shkotovo Pl	Bikin Pl	Nelma Pl	Sovgavan Pl
Rock name:	alkali basalt	basanite	ol tholeiite	ol tholeiite	ol tholeiite	ol tholeiite	ol tholeiite	ol tholeiite
(wt %)								
SiO_2	47·82	48·99	50·95	51·93	51·06	49·65	49·94	49·36
TiO_2	1·83	1·90	2·19	1·41	1·89	2·23	2·18	1·75
Al_2O_3	15·87	16·73	17·64	15·92	15·35	15·85	14·46	15·28
FeO^*	9·64	9·16	11·14	11·43	11·73	10·20	12·19	11·31
MnO	0·18	0·16	0·09	0·13	0·17	0·15	0·14	0·14
MgO	8·48	6·96	3·93	6·83	6·14	7·10	7·04	7·96
CaO	8·31	7·32	5·18	8·00	6·70	8·13	7·87	8·45
Na_2O	3·43	4·26	3·94	3·44	3·69	3·67	3·70	3·41
K_2O	2·19	2·28	3·21	0·17	1·74	0·96	0·99	1·06
P_2O_5	0·54	0·62	0·90	0·17	0·47	0·47	0·37	0·34
Total	98·29	98·38	99·17	99·43	98·94	98·41	98·88	99·06
XRF trace elements (ppm)								
Ni		148	60		120	148	140	
Cr		240	49		132	187	211	
Co		35	37		51	42	54	
Cu		43	30		52	40	38	
Zn		75	109		117	117	118	
V		146	139		182	173	196	
Zr		234	232		158	167	127	
ICP–MS trace elements (ppm)								
Ni	161			183				188
Cr	259			220				257
Co	52			54				58
Sc	17·3	18·8	13·1	17·8	19·6	19·3	23·6	19·8
Cu	42			65				61
Zn	78			116				101
V	174			191				199
Y	20·81	25·87	25·26	19·11	27·92	23·68	27·60	15·47
Ga	17·1			22·1				19·9
Rb	48·1	71·7	73·1	1·2	28·6	9·9	9·3	21·5
Sr	935	829	876	474	387	641	483	500
Ba	944	747	1274	100	458	517	372	320
Zr	200			71				94
Hf	4·30	5·43	4·90	1·74	3·93	4·02	3·47	2·70
Nb	72·31	61·16	57·26	4·59	30·53	31·08	25·41	14·60
Ta	3·35	3·94	3·38	0·31	1·38	1·94	1·49	1·12
Th	4·87	6·87	5·60	0·68	2·96	3·00	2·81	1·88
U	1·12	1·59	1·14	0·12	0·63	0·35	0·50	0·57
Pb	3·99	5·94	4·49	1·84	2·16	2·59	2·46	2·65
Cs	0·57	1·38	0·44	0·07	0·18	0·16	0·08	1·08

	Mid-Miocene—Pliocene (14—5 Ma)							
Sample no.:	YuM1381[1]	YuM1328[2]	Yu84[2]	YuS108/10[1]	P369/13[2]	SO-36[2]	YuM1787[2]	YuS108/6[1]
Age (Ma):[3]	9·9	11·9			8·7	5·0	5·4	8·1
Locality:	Koppi riv.	Koppi riv.	Sovgavan Pl	Sovgavan Pl	Shkotovo Pl	Bikin Pl	Nelma Pl	Sovgavan Pl
Rock name:	alkali basalt	basanite	ol tholeiite	ol tholeiite	ol tholeiite	ol tholeiite	ol tholeiite	ol tholeiite
Mo	1·8			0·4				0·7
Li	7·5			8·6				7
La	51·64	45·08	45·14	4·92	27·73	22·67	21·28	14·22
Ce	99·92	78·25	74·51	12·29	46·15	44·09	38·66	30·32
Pr	9·63	8·51	8·38	1·96	5·89	5·53	4·79	3·92
Nd	34·76	34·15	36·86	10·22	25·49	24·92	21·54	16·61
Sm	6·00	7·20	8·01	3·28	6·89	6·80	6·12	3·98
Eu	1·97	2·23	2·73	1·21	2·34	2·41	2·20	1·39
Tb	0·77	0·94	1·01	0·54	1·05	0·97	0·99	0·61
Gd	5·52	6·01	6·82	3·58	6·87	6·35	6·37	4·10
Dy	3·81	5·25	5·33	3·08	5·99	5·50	5·82	3·35
Ho	0·73	0·97	0·96	0·60	1·09	0·93	1·04	0·66
Er	1·96	2·45	2·22	1·59	2·60	2·19	2·54	1·73
Tm		0·34	0·31		0·34	0·29	0·33	
Yb	1·69	2·12	1·82	1·29	2·02	1·58	1·92	1·44
Lu	0·25	0·32	0·27	0·19	0·30	0·23	0·29	0·21

	Mid-Miocene—Pliocene (14—5 Ma)							
Sample no.:	P369/11[1]	P369/11b[1]	SO-29[1]	YuM1120[1]	YuS120/9[1]	P369/2[1]	VS-1[1]	VS-3[2]
Age (Ma):[3]	10·8	8·9	6·4	6·4		11·8		
Locality:	Shkotovo Pl	Shkotovo Pl	Nelma Pl	Nelma Pl	Sovgavan Pl	Shkotovo Pl	Shufan Pl	Shufan Pl
Rock name	ol tholeiite	ol tholeiite	qz tholeiite	qz tholeiite	qz tholeiite	qz tholeiite	qz tholeiite	qz tholeiite
(wt %)								
SiO_2	51·69	49·29	52·57	53·62	53·97	54·46	55·56	53·25
TiO_2	1·76	1·37	1·82	1·64	1·51	1·55	1·80	2·89
Al_2O_3	15·63	16·72	15·22	16·57	15·79	14·79	14·98	14·09
FeO^*	9·86	11·54	9·86	9·40	8·94	9·98	8·98	12·35
MnO	0·15	0·18	0·15	0·15	0·14	0·14	0·12	0·15
MgO	6·12	7·29	6·72	4·90	5·54	6·59	6·56	4·59
CaO	7·86	8·63	7·79	7·23	8·50	7·49	7·66	6·87
Na_2O	3·53	3·06	3·52	3·26	3·86	3·09	3·09	3·04
K_2O	1·75	0·31	0·93	2·11	0·16	0·44	0·90	1·74
P_2O_5	0·43	0·15	0·29	0·75	0·20	0·18	0·27	0·67
Total	98·78	98·54	98·87	99·63	98·61	98·81	99·92	99·64
XRF trace elements (ppm)								
Ni								107
Cr								129
Co								49

Table 2: continued

	Mid-Miocene—Pliocene (14–5 Ma)							
Sample no.:	P369/11[1]	P369/11b[1]	SO-29[1]	YuM1120[1]	YuS120/9[1]	P369/2[1]	VS-1[1]	VS-3[2]
Age (Ma):[3]	10·8	8·9	6·4	6·4		11·8		
Locality:	Shkotovo Pl	Shkotovo Pl	Nelma Pl	Nelma Pl	Sovgavan Pl	Shkotovo Pl	Shufan Pl	Shufan Pl
Rock name:	ol tholeiite	ol tholeiite	qz tholeiite	qz tholeiite	qz tholeiite	qz tholeiite	qz tholeiite	qz tholeiite
Cu								39
Zn								115
V								201
Zr								189
ICP–MS trace elements (ppm)								
Ni	121	145	175	137	151	148	183	
Cr	207	239	218	159	282	261	234	
Co	53	66	62	51	47	51	47	
Sc	20·3	21·0	19·3	17·5	17·2	17·4	15·6	20·2
Cu	48	44	58	60	48	41	64	
Zn	122	97	113	106	112	107	107	
V	198	170	169	167	160	162	161	
Y	20·79	18·56	25·67	22·68	21·47	19·86	18·91	26·31
Ga	20·7	19·2	22·1	20·4	22·7	20·4	20·5	
Rb	34·2	2·4	18·5	29·4	4·9	6·1	13·9	29·5
Sr	593	235	536	595	409	285	553	676
Ba	358	129	270	424	103	155	200	527
Zr	147	101	134	132	78	83	105	
Hf	3·43	2·26	3·03	3·19	1·90	2·18	2·50	5·06
Nb	31·22	12·17	18·50	22·36	4·37	7·35	5·08	12·03
Ta	2·01	0·98	1·13	1·36	0·30	0·52	0·40	0·74
Th	3·82	1·87	1·43	1·97	0·44	1·06	0·81	1·69
U	0·97	0·38	0·34	0·48	0·10	0·21	0·21	0·36
Pb	4·16	2·27	1·96	2·42	1·28	1·93	2·44	3·74
Cs	0·26	0·15	0·28	0·44	0·19	0·09	0·20	0·35
Mo	1·5	0·8	1·2	1·4	0·5	0·4	0·6	
Li	10·5	9·3	5·5	6·3	6·0	5·3	8·4	
La	26·28	7·66	12·18	15·20	6·15	7·12	8·40	21·13
Ce	56·11	16·10	28·57	31·88	14·83	14·12	18·72	45·85
Pr	5·94	2·16	3·72	4·31	2·45	2·25	2·98	6·17
Nd	23·08	9·25	17·46	19·45	13·25	11·58	14·69	30·46
Sm	4·92	2·63	4·96	5·12	4·28	3·94	4·24	8·47
Eu	1·65	1·01	1·76	1·77	1·56	1·47	1·55	2·81
Tb	0·73	0·50	0·78	0·78	0·68	0·64	0·61	1·05
Gd	4·99	3·06	5·22	5·32	4·65	4·38	4·27	7·14
Dy	3·88	3·07	4·26	4·15	3·73	3·55	3·24	5·56
Ho	0·75	0·62	0·81	0·79	0·71	0·66	0·60	0·99
Er	1·95	1·69	2·06	1·99	1·80	1·68	1·52	2·24
Tm								0·29
Yb	1·58	1·48	1·63	1·58	1·36	1·30	1·19	1·68
Lu	0·23	0·21	0·23	0·22	0·19	0·18	0·17	0·24

	Early-Mid—Miocene (23—15 Ma)						*Eocene—Oligocene (55—24 Ma)*	
Sample no.:	Yu17	Yu19[1]	S-11[2]	SA-02[2]	SA-04[2]	S-3[2]	YuM609[1]	Yu770[2]
Age (Ma):[3]		21·1	16·9				36·8	24·8
Locality:	Sovgavan	Sovgavan	Sakhalin	Sakhalin	Sakhalin	Sakhalin	Low Amur	Low Amur
Rock name:	ol tholeiite	ol tholeiite	ol tholeiite	ol tholeiite	qz tholeiite	qz tholeiite	ol tholeiite	ol tholeiite
(wt %)								
SiO_2	49·65	48·87	47·7	46·91	50·49	51·9	54·01	49·6
TiO_2	0·86	0·86	0·90	1·05	0·71	0·92	1·14	1·55
Al_2O_3	18·61	17·68	19·32	19·95	19·21	17·42	17·46	17·46
FeO^*	9·39	10·99	10·33	10·54	9·23	8·25	8·05	10·03
MnO	0·19	0·17	0·20	0·19	0·21	0·17	0·15	0·19
MgO	5·90	6·25	5·60	4·32	4·42	4·58	5·09	6·57
CaO	11·29	10·67	12·18	12·92	10·81	11·42	7·41	8·28
Na_2O	2·52	2·36	2·23	2·25	2·53	2·84	3·74	3·16
K_2O	0·82	0·75	0·65	0·33	0·31	0·36	2·01	1·57
P_2O_5	0·17	0·15	0·09	0·14	0·14	0·18	0·45	0·40
Total	99·39	98·75	99·20	98·60	98·06	98·04	99·51	98·81
XRF trace elements (ppm)								
Ni	26		7		14			70
Cr	59		11		23			84
Co	33		37		33			39
Cu	54		96		41			30
Zn	75		61		81			83
V	279		379		252			214
Zr	54		18		39			148
ICP—MS trace elements (ppm)								
Ni		54					68	
Cr		78					113	
Co		53					61	
Sc		32·9	48·3	460	30·4	32·7	22·0	29·0
Cu		81					65	
Zn		70					81	
V		330					211	
Y		18·85	15·22	23·09	17·19	25·00	21·08	28·08
Ga		17·6					19·4	
Rb		7·9	6·4	1·8	9	3·5	46	22
Sr		610	362	381	383	342	724	947
Ba		175	164	151	159	143	640	316
Zr		47					132	
Hf		1·24	0·71	1·37	1·21	2·02	3·59	2·91
Nb		1·53	0·46	1·91	1·58	2·03	9·39	11·63
Ta		0·22	0·03	0·11	0·09	0·14	0·99	0·66
Th		1·24	0·83	1·09	1·05	0·60	3·78	1·31
U		0·31	0·26	0·32	0·36	0·21	1·05	0·34
Pb		5·27	3·42	3·98	5·53	5·32	10·48	5·22
Cs		0·22	0·6	0·07	0·99	0·23	2·05	0·26

Table 2: continued

	Early Mid—Miocene (23–15 Ma)						Eocene—Oligocene (55–24 Ma)	
Sample no.:	Yu17	Yu19[1]	S-11[2]	SA-02[2]	SA-04[2]	S-3[2]	YuM609[1]	Yu770[2]
Age (Ma):[3]		21·1	16·9				36·8	24·8
Locality:	Sovgavan	Sovgavan	Sakhalin	Sakhalin	Sakhalin	Sakhalin	Low Amur	Low Amur
Rock name:	ol tholeiite	ol tholeiite	ol tholeiite	ol tholeiite	qz tholeiite	qz tholeiite	ol tholeiite	ol tholeiite
Mo		0·5					1·3	
Li		7·2					16·8	
La		6·14	3·68	5·12	6·07	5·64	25·1	15·44
Ce		14·55	8·34	12·45	13·12	13·35	52·94	32·02
Pr		2·07	1·14	1·77	1·76	1·91	6·67	4·12
Nd		9·52	5·83	9·14	8·50	9·50	26·67	19·21
Sm		2·64	2·05	2·98	2·50	3·19	5·55	5·24
Eu		0·86	0·78	1·14	0·92	1·05	1·60	1·87
Tb		0·45	0·43	0·66	0·49	0·68	0·75	0·87
Gd		2·77	2·39	3·63	2·73	3·78	5·25	5·10
Dy		2·79	2·87	4·26	3·14	4·44	4·14	5·31
Ho		0·61	0·61	0·87	0·66	0·94	0·86	1·05
Er		1·79	1·74	2·64	1·77	2·61	2·44	2·78
Tm			0·24	0·37	0·26	0·38		0·39
Yb		1·70	1·48	2·28	1·74	2·35	2·34	2·50
Lu		0·26	0·23	0·35	0·27	0·38	0·35	0·39

	Eocene—Oligocene (55–24 Ma)							
Sample no.:	YuM537	Yu155/1B[2]	Yu-S122/7	YuS122/8[2]	YuS122/13[1]	YuS122/14[1]	Yu7[2]	SO-13[1]
Age (Ma):[3]	36·7	31·5	24·4			29		34·7
Locality:	Low Amur	Low Amur	Sovgavan	Sovgavan	Sovgavan	Sovgavan	Sovgavan	Nelma
Rock name:	ol tholeiite	ol tholeiite	ol tholeiite	qz tholeiite	ol tholeiite	ol tholeiite	ol tholeiite	ol tholeiite
(wt %)								
SiO_2	48·66	52·21	52·05	52·29	52·62	52·43	52·25	48·37
TiO_2	1·41	1·40	1·25	1·04	1·20	1·31	1·89	2·36
Al_2O_3	16·77	17·46	19·27	21·42	19·58	17·86	17·96	15·28
FeO^*	10·17	9·34	8·53	8·76	7·76	8·26	9·31	11·68
MnO	0·15	0·17	0·14	0·17	0·14	0·14	0·13	0·21
MgO	6·76	5·41	4·96	4·69	4·62	0·30	4·62	4·67
CaO	8·47	7·96	8·66	7·26	6·92	7·73	6·86	8·25
Na_2O	3·41	3·45	3·85	3·42	4·23	3·81	4·23	3·06
K_2O	1·29	1·61	0·67	0·77	1·40	1·24	1·88	1·33
P_2O_5	0·49	0·53	0·37	0·45	0·35	0·48	0·56	1·33
Total	97·58	99·54	99·65	100·27	98·72	99·61	99·69	98·54
XRF trace elements (ppm)								
Ni	94	80	42				52	33
Cr	100	113	56				70	73
Co	41	34	29·9				38	26

	Eocene—Oligocene (55—24 Ma)							
Sample no.:	YuM537	Yu155/1B[2]	Yu-S122/7	YuS122/8[2]	YuS122/13[1]	YuS122/14[1]	Yu7[2]	SO-13[1]
Age (Ma):[3]	36·7	31·5	24·4			29		34·7
Locality:	Low Amur	Low Amur	Sovgavan	Sovgavan	Sovgavan	Sovgavan	Sovgavan	Nelma
Rock name.	ol tholeiite	ol tholeiite	ol tholeiite	qz tholeiite	ol tholeiite	ol tholeiite	ol tholeiite	ol tholeiite
Cu	58	77	47·9				38	27
Zn	85	95	84				72	140
V	210	210	202				181	209
Zr	135	153	125				210	229
ICP—MS trace elements (ppm)								
Ni					57	110		35
Cr					67	177		84
Co					38	56		35
Sc		26·8		29·2	18·3	17·8	21·6	21·4
Cu					118	46		44
Zn					83	80		140
V					216	172		236
Y		29·45		33·86	16·97	20·29	26·36	36·52
Ga					20·3	17·9		20·7
Rb		23·9		7·7	14·7	11·4	18·8	10·6
Sr		698		485	825	790	711	870
Ba		493		462	351	250	375	648
Zr					110	146		250
Hf		3·36		4·84	2·91	3·39	4·48	5·13
Nb		11·57		20·29	9·70	12·57	19·52	23·53
Ta		0·63		1·29	0·73	1·1	1·30	1·08
Th		1·89		2·42	1·57	1·58	1·87	1·48
U		0·49		0·80	0·47	0·45	0·60	0·39
Pb		10·90		9·15	8·10	7·93	6·11	10·11
Cs		0·64		0·21	0·30	0·23	0·17	0·20
Mo					1·0	1·3		1·1
Li					12·5	9·5		13·7
La		22·14		27·50	15·63	16·18	24·97	37·75
Ce		45·27		56·51	34·45	35·53	46·98	105·91
Pr		5·73		6·90	4·35	4·56	5·80	12·26
Nd		25·56		29·10	18·16	18·75	24·99	51·60
Sm		6·18		7·12	4·02	4·16	5·79	10·74
Eu		1·90		2·36	1·32	1·32	1·96	2·88
Tb		0·93		1·09	0·60	0·63	0·85	1·27
Gd		5·79		6·70	4·00	4·17	5·42	9·55
Dy		5·61		6·66	3·35	3·61	4·83	6·29
Ho		1·11		1·28	0·69	0·75	0·95	1·20
Er		2·90		3·50	1·93	2·14	2·49	3·17
Tm		0·41		0·49			0·35	
Yb		2·63		3·12	1·77	2·02	2·10	2·70
Lu		0·41		0·49	0·27	0·31	0·33	0·40

Table 2: continued

	Eocene—Oligocene (55—24 Ma)							
Sample no.:	SO-17	SO-9[2]	SO-23[1]	YuM1119[1]	K-01[1]	SO-62[2]	S-12A[2]	S-17[2]
Age(Ma):[3]	36·1	33·6	33·6	34·9	47·3	54·8	38·7	30·7
Locality:	Nelma	Nelma	Nelma	Samarga riv.	Kavalerovo	Nakhodka	Sakhalin	Sakhalin
Rock name:	ol tholeiite	qz tholeiite	qz tholeiite	qz tholeiite	qz tholeiite	qz tholeiite	qz tholeiite	qz tholeiite
(wt %)								
SiO_2	52·53	51·42	51·52	52·92	52·01	53·75	54·64	52·53
TiO_2	1·62	1·68	1·84	1·59	1·88	1·33	0·95	1·62
Al_2O_3	17·27	17·05	15·96	16·38	17·96	17·83	17·82	17·27
FeO^*	9·18	9·51	9·65	9·46	8·37	7·34	7·04	9·18
MnO	0·16	0·18	0·18	0·19	0·14	0·14	0·10	0·16
MgO	4·69	5·39	5·59	4·49	4·39	3·72	6·17	4·69
CaO	7·23	8·13	7·86	6·99	8·68	8·05	7·71	7·23
Na_2O	3·57	3·42	3·40	3·11	3·50	3·86	3·55	3·57
K_2O	1·94	1·14	1·35	1·97	1·49	1·83	1·05	1·94
P_2O_5	0·70	0·79	1·08	0·65	0·72	0·48	0·31	0·70
Total	98·89	98·71	98·43	97·75	99·14	98·33	99·34	98·89
XRF trace elements (ppm)								
Ni		57				55	134	43
Cr		105				63	198	86
Co		28				28	40	26
Cu		24				17	50	39
Zn		114				81	56	110
V		205				145	168	200
Zr		191				235	117	216
ICP—MS trace elements (ppm)								
Ni			84	54	62			
Cr			129	83	136			
Co			34	34	32			
Sc		21·1	19·8	17·6	19·9	19·9	20·8	20·1
Cu			41	39	31			
Zn			115	106	95			
V			197	204	206			
Y		26·28	32·41	27·37	22·07	25·39	18·62	18·69
Ga			19·4	19·1	20·8			
Rb		18·4	19·8	39·3	16·1	49·3	8·2	6·7
Sr		835	812	766	861	755	727	651
Ba		526	567	661	626	576	276	279
Zr			248	164	182			
Hf		4·39	5·09	3·42	4·29	5·24	2·63	2·56
Nb		13·77	20·57	11·10	11·77	14·82	7·71	7·81
Ta		0·73	0·96	0·54	0·77	0·89	0·51	0·49
Th		4·33	1·93	3·78	4·03	5·09	0·90	0·96
U		0·92	0·53	1·09	0·91	0·98	0·26	0·29
Pb		12·49	10·81	11·73	9·71	9·17	4·98	7·47
Cs		0·72	0·92	0·81	0·96	3·43	0·24	0·10
Mo			1·3	1·1	0·6			

	Eocene—Oligocene (55—24 Ma)							
Sample no.:	SO-17	SO-9[2]	SO-23[1]	YuM1119[1]	K-01[1]	SO-62[2]	S-12A[2]	S-17[2]
Age(Ma):[3]	36·1	33·6	33·6	34·9	47·3	54·8	38·7	30·7
Locality:	Nelma	Nelma	Nelma	Samarga riv.	Kavalerovo	Nakhodka	Sakhalin	Sakhalin
Rock name:	ol tholeiite	qz tholeiite	qz tholeiite	qz tholeiite	qz tholeiite	qz tholeiite	qz tholeiite	qz tholeiite
Li			11·3	17·9	6·3			
La		31·96	35·69	23·04	24·45	34·01	12·41	12·24
Ce		68·44	96·06	62·27	65·48	69·50	26·42	25·81
Pr		8·31	11·04	6·89	7·01	7·86	3·26	3·13
Nd		36·32	45·67	28·57	28·83	31·58	14·22	14·53
Sm		8·34	9·26	6·08	6·02	6·86	3·69	3·61
Eu		2·43	2·41	1·79	1·96	2·01	1·24	1·25
Tb		0·99	1·10	0·79	0·80	0·88	0·58	0·57
Gd		6·58	8·20	5·60	5·66	5·69	3·57	3·55
Dy		5·62	5·49	4·17	4·20	5·14	3·53	3·46
Ho		1·02	1·06	0·83	0·84	0·98	0·71	0·71
Er		2·49	2·82	2·26	2·28	2·51	1·89	1·84
Tm		0·35				0·36	0·27	0·26
Yb		2·15	2·45	2·02	2·04	2·17	1·71	1·69
Lu		0·32	0·36	0·30	0·30	0·35	0·27	0·26

	Mudanjian	*Standard rock*	
Sample no.:	J-8[2]	BCR-2[4]	BIR-1[5]
Age (Ma):[3]	8·5[6]		
Locality:	NE China		
Rock name:	basanite		
(wt %)			
SiO_2	45·37		
TiO_2	2·28		
Al_2O_3	14·88		
FeO^*	10·73		
MnO	0·16		
MgO	9·64		
CaO	9·01		
Na_2O	3·51		
K_2O	1·94		
P_2O_5	0·68		
Total	98·20		
XRF trace elements (ppm)			
Ni	173		
Cr	269		
Co	52		
Cu	42		
Zn	89		
V	178		
Zr	213		

Table 2: continued

	Mudanjian	*Standard rock*	
Sample no.:	J-8[2]	BCR-2[4]	BIR-1[5]
Age (Ma):[3]	8·5[6]		
Locality:	NE China		
Rock name:	basanite		
ICP—MS trace elements (ppm)			
Ni			
Cr			
Co			
Sc	22·1		
Cu			117 ± 3
Zn			68 ± 2
V			
Y	21·83	38·11 ± 0·29	16·6 ± 0·3
Ga			
Rb	17·5	48·06 ± 0·67	0·23 ± 0·02
Sr	887		110 ± 2
Ba	270	670·50 ± 12·68	6·75 ± 0·08
Zr			15·3 ± 0·2
Hf	4·60	4·67 ± 0·07	0·042 ± 0·002
Nb	49·94	13·31 ± 0·29	0·57 ± 0·01
Ta	3·25	0·82 ± 0·02	2·7 ± 0·2
Th	3·65	5·13 ± 0·49	0·039 ± 0·005
U	1·14	1·15 ± 0·11	0·0111 ± 0·0006
Pb	2·85	9·11 ± 0·29	
Cs	0·38	0·96 ± 0·03	
Mo			
Li			
La	32·53	26·26 ± 0·49	0·69 ± 0·06
Ce	61·61	51·67 ± 0·62	1·88 ± 0·02
Pr	7·02	6·32 ± 0·06	0·376 ± 0·003
Nd	29·53	27·36 ± 0·48	2·37 ± 0·03
Sm	6·98	7·03 ± 0·15	1·10 ± 0·01
Eu	2·35	2·14 ± 0·04	0·52 ± 0·01
Tb	0·90	1·17 ± 0·01	1·78 ± 0·02
Gd	6·28	6·75 ± 0·08	0·351 ± 0·005
Dy	4·92	7·14 ± 0·10	2·52 ± 0·03
Ho	0·87	1·44 ± 0·02	0·586 ± 0·007
Er	1·95	4·05 ± 0·06	1·73 ± 0·03
Tm	0·25	0·55 ± 0·01	1·61 ± 0·02
Yb	1·39	3·36 ± 0·03	0·252 ± 0·008
Lu	0·20	0·52 ± 0·01	0·577 ± 0·007

[1]ICP-MS data obtained in the Macquarie University Geochemical Analysis Unit.
[2]ICP-MS data obtained in the Geoanalytical Laboratory of Washington State University.
[3]Okamura *et al.* (1998*b*).
[4]Average of 50 analyses on rock standards at Washington State University.
[5]Average of 33 analyses on rock standards at Macquarie University.
[6]Okamura *et al.* (unpublished data).
Total Fe as FeO.

Table 3: Sr–Nd–Pb isotopic data for Sikhote-Alin–Sakhalin volcanic rocks

Sample	Age (Ma)	Rb (ppm)	Sr (ppm)	$^{87}Sr/^{86}Sr$ measured	$^{87}Sr/^{86}Sr$ initial	Sm (ppm)	Nd (ppm)	$^{143}Nd/^{144}Nd$ measured	$^{143}Nd/^{144}Nd$ initial	$^{206}Pb/^{204}Pb$	$^{207}Pb/^{204}Pb$	$^{208}Pb/^{204}Pb$
Mid-Miocene–Pliocene (14–5 Ma)												
YuM1381	9·9	48·1	935	0·703710	0·703689	6·00	34·76	0·512677	0·512662	18·350	15·481	38·664
YuM1328	11·9	71·7	329	0·704362	0·704320	7·20	34·15	0·512804	0·512794			
Yu84	7	73·1	876	0·703840	0·703816	8·01	36·86	0·512714	0·512708			
YuS108/10	8	1·2	474	0·703926	0·703925	3·28	10·22	0·512574	0·512564			
P369/13	8·7	28·6	387	0·704488	0·704462	6·89	25·49	0·512684	0·512675			
SO-36	5·0	9·9	641	0·704085	0·704082	6·80	24·92	0·512743	0·512738			
YuM1787	5·4	9·3	483	0·704243	0·704239	6·12	21·54	0·512727	0·512721			
YuS108/6	8·1	21·5	500	0·704126	0·704112	3·98	16·61	0·512647	0·512639	17·687	15·497	37·734
P369/11	10·8	34·2	593	0·704289	0·704263	4·92	23·08	0·512692	0·512683	18·056	15·547	38·166
P369/11b	8·9	2·4	235	0·704480	0·704476	2·63	9·25	0·512791	0·512781	18·324	15·556	38·435
SO-29	6·4	18·5	536	0·703853	0·703844	4·96	17·46	0·512815*	0·512808			
YuM1120	6·4	29·4	595	0·703859	0·703846	5·12	19·45	0·512705	0·512698	17·880	15·560	38·005
YuS120/9	8	4·9	409	0·704325	0·704321	4·28	13·25	0·512496	0·512486	17·299	15·490	37·288
P369/2	11·8	6·1	285	0·704693	0·704683	3·94	11·58	0·512649	0·512633	17·970	15·558	38·087
VS-1	10	13·9	553	0·704152	0·704142	4·24	14·69	0·512716	0·512705	17·266	15·481	37·109
VS-3	10	29·5	676	0·704757	0·704739	8·47	30·46	0·512623	0·512612	17·308	15·514	37·353
Early–Mid-Miocene (23–15 Ma)												
Yu17*	21	16·0	594	0·703434	0·703411	3·00	11·36	0·512918	0·512896			
Yu19	21·1	7·9	610	0·703359	0·703348	2·54	9·52	0·512905	0·512883	18·218	15·520	38·185
S-11	16·9	6·4	362	0·703634	0·703622	2·05	5·83	0·512942	0·512919			
SA-04	17	9·0	383	0·703650	0·703634	2·50	8·50	0·512922	0·512902			
Eocene–Oligocene (55–24 Ma)												
YuM609	36·8	46·0	724	0·704030	0·703934	5·55	26·67	0·512844	0·512814	18·472	15·605	38·550
Yu770	24·8	22·0	947	0·703896	0·703872	5·24	19·21	0·512886	0·512859			
YuM537*	36·7	31·0	649	0·703945	0·703873			0·512787				
Yu155/1B	31·5	23·9	698	0·703892	0·703848	6·18	25·56	0·512836	0·512806			
YuS122/7*	24·4	19·0	761	0·703955	0·703930	4·63	21·34	0·512827	0·512806			
YuS122/9	24	7·7	485	0·703733	0·703717	7·12	29·10	0·512902	0·512879			

Table 3: continued

Sample	Age (Ma)	Rb (ppm)	Sr (ppm)	$^{87}Sr/^{86}Sr$ measured	$^{87}Sr/^{86}Sr$ initial	Sm (ppm)	Nd (ppm)	$^{143}Nd/^{144}Nd$ measured	$^{143}Nd/^{144}Nd$ initial	$^{206}Pb/^{204}Pb$	$^{207}Pb/^{204}Pb$	$^{208}Pb/^{204}Pb$
YuS122/13	29	14·7	825	0·703874	0·703853	4·02	18·16	0·512846	0·512821	18·293	15·533	38·262
YuS122/14	29·0	11·4	790	0·703771	0·703754	4·16	18·75	0·512881	0·512856	18·259	15·538	38·245
Yu7	25	18·8	711	0·703699	0·703672	5·79	24·99	0·512900	0·512877			
SO-13	34·7	10·6	870	0·704563	0·704546	10·74	51·60	0·512669	0·512640	18·384	15·523	38·435
SO-17*	36·1	33·4	744	0·704378	0·704311			0·512755				
SO-9	33·6	18·4	835	0·704467	0·704437	8·34	36·32	0·512683	0·512653			
SO-23	33·6	19·8	812	0·704438	0·704404	9·26	45·67	0·512732	0·512705	18·370	15·545	38·395
YuM1119	34·9	39·3	766	0·704806	0·704732	6·08	28·57	0·512738	0·512709	18·478	15·645	38·749
K-01	47·3	16·1	861	0·705097	0·705061	6·02	28·83	0·512647	0·512608	18·398	15·573	38·508
SO-62	54·8	49·3	755	0·705157	0·705010	6·86	31·58	0·512662	0·512615			
S-12A	38·7	8·2	727	0·704155	0·704137	3·69	14·22	0·512861	0·512821			
S-17	30·7	6·7	651	0·703906	0·703893	3·61	14·53	0·512845	0·512815			

*Element concentrations in samples are from isotope dilution method.

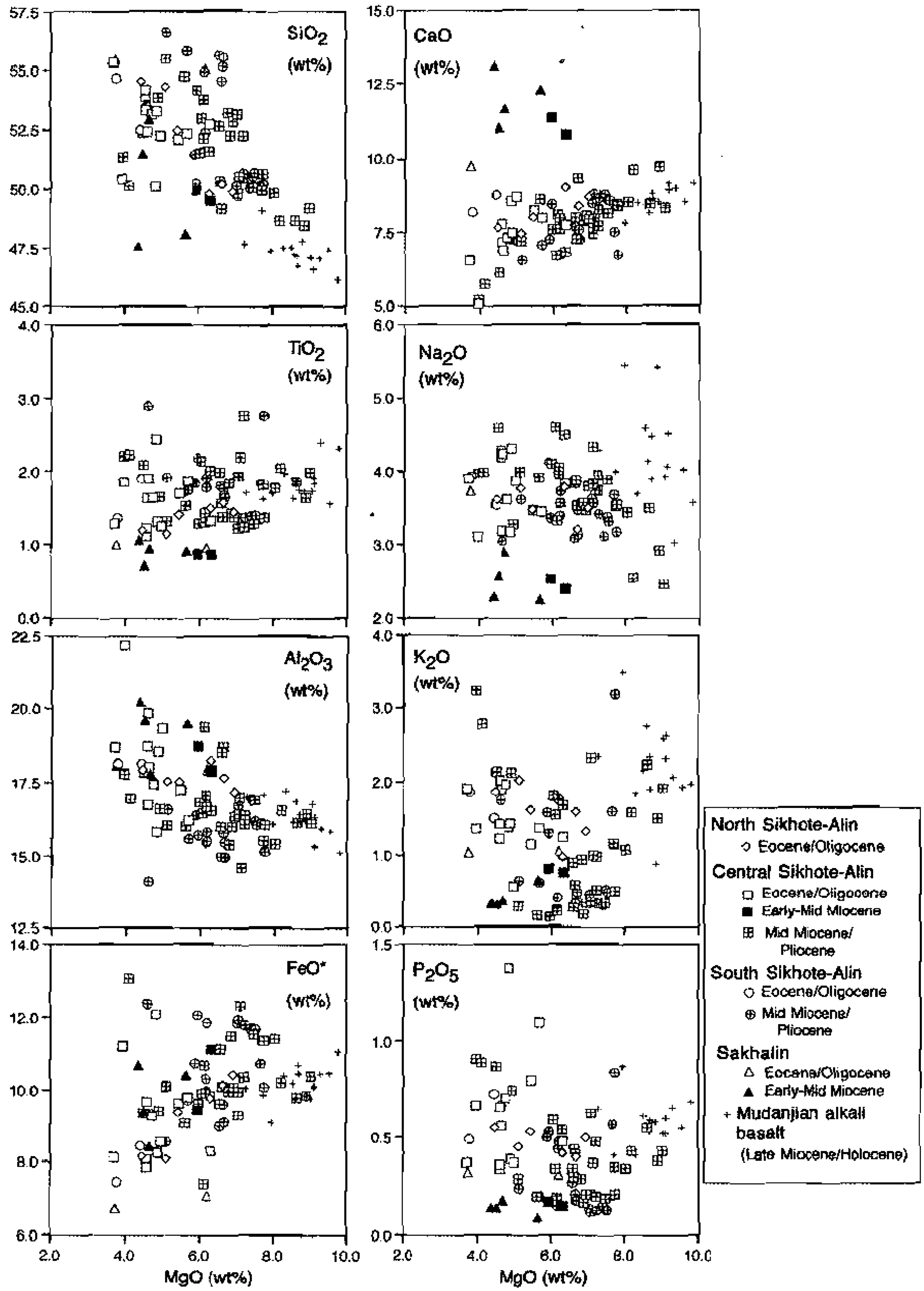

Fig. 4. Wt % MgO vs wt % SiO_2, TiO_2, Al_2O_3, total Fe as FeO*, CaO, Na_2O, K_2O and P_2O_5 for the volcanic rocks of the Sikhote-Alin–Sakhalin and Mudanjian area.

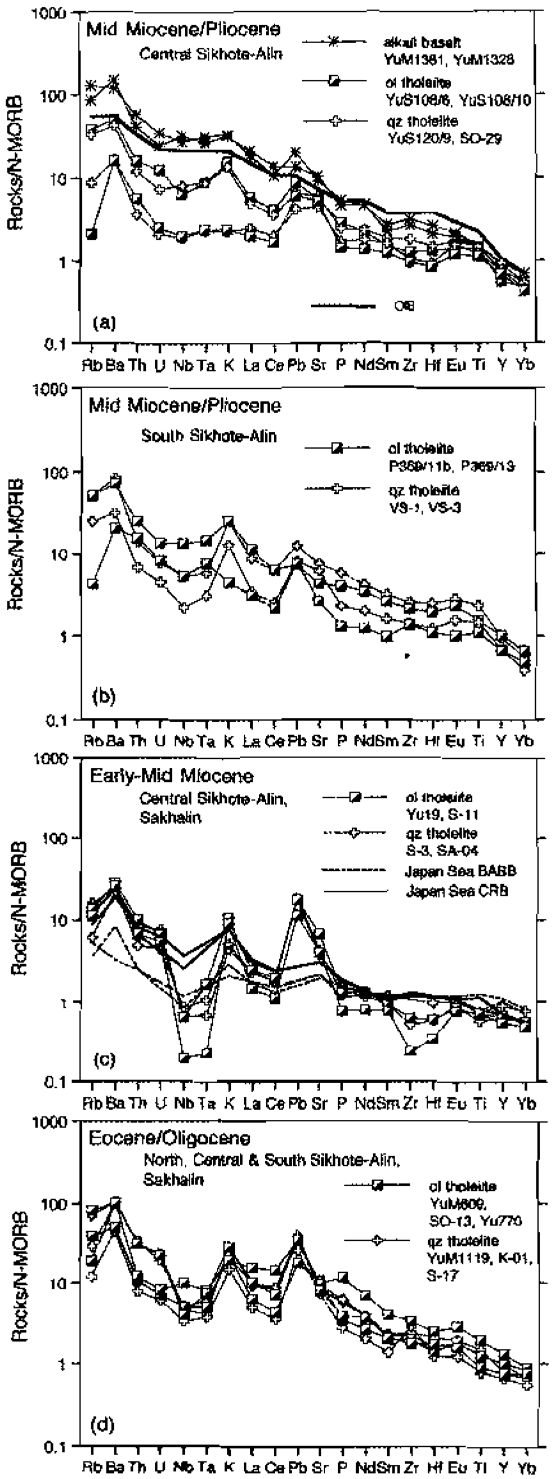

Fig. 5. N-MORB-normalized incompatible element diagrams for: (a) Mid-Miocene–Pliocene basalts from central Sikhote-Alin; (b) Mid-Miocene–Pliocene basalts from south Sikhote-Alin; (c) Early–Mid-Miocene basalts from central Sikhote-Alin–Sakhalin; (d) Eocene–Oligocene basalts from north, central and south Sikhote-Alin and Sakhalin. Japan Sea BABB (back-arc basin basalts) and Japan Sea CRB continental rift tholeiites; from Pouclet *et al.* (1995). Normalizing values from Sun & McDonough (1989).

Sikhote-Alin have Nb and Ta depletions relative to K, and more closely resemble the trace-element patterns of the Eocene–Oligocene basalts (Fig. 5b). The trace-element characteristics of spinel lherzolite xenoliths from Sikhote-Alin are very different from those of their host Mid-Miocene–Pliocene alkali basalts (Fig. 6). The Sikhote-Alin peridotites have distinctively low contents of Th, U, Nb and Ta relative to LREE (Ionov *et al.*, 1995). The general shape of the xenolith trace-element patterns is not similar to that of the host basalt and other volcanic rocks from Sikhote-Alin and Sakhalin region. These features indicate no genetic relationships of the peridotites with their host volcanic rocks.

Chondrite-normalized REE patterns for the Mid-Miocene–Pliocene basalts vary with the magma type, with LREE enrichment increasing systematically from quartz and olivine tholeiites to alkali basalt types (Fig. 7a). The Early–Mid-Miocene tholeiites have flatter REE profiles, similar to those of MORB. REE enrichment appears to pivot about Dy–Tb in the Eocene–Oligocene basalts and the Mid-Miocene–Pliocene basalts (Fig. 7a and c). Heavy REE (HREE; Dy–Lu) abundances and $(Dy/Yb)_N$ ratios are thus essentially identical for all types and show no variation with the degree of SiO_2-saturation. The Mid-Miocene–Pliocene basalts have a variable range in La/Yb and Tb/Yb, but on average, much lower ratios than the Hannuoba alkali basalts (Fig. 8). The systematically different La/Yb, similar HREE abundances and the absence of HREE depletion in Fig. 7 (expected from melting of garnet lherzolite) suggest that partial melting of a spinel lherzolite mantle source occurred beneath the Sikhote-Alin and Sakhalin region. Lavas from the intraplate Hannuoba alkali basalts are strongly enriched in both La and Tb relative to Yb (Zhi *et al.*, 1990), suggesting melt generation from a garnet-bearing source. The similar La abundances but systematically higher Yb abundances and lower La/Yb in the Mid-Miocene–Pliocene alkali basalts relative to the Hannuoba alkali basalts are best modeled by similar (small percent) extents of melting of a spinel lherzolite mantle source.

Figure 9 illustrates the variation of Zr/Y with Zr/Nb. The wide range of incompatible-element abundances in the Sikhote-Alin and Sakhalin basalts defines a hyperbolic trend consistent with mixing of mantle sources of different composition. The Mid-Miocene–Pliocene basalts appear to show a coherent relationship. A mixing hyperbola is illustrated, calculated using the most extreme basalt compositions and the equations of Langmuir *et al.* (1978). The data correspond well to the predicted mixing curve. Extrapolation of the mixing hyperbola towards lower Zr/Nb intersects the field of basalts from Hannuoba (Zhi *et al.*, 1990) and Mudanjian. Extrapolation towards higher Zr/Nb ratios provides a compositional range for the other end-member with

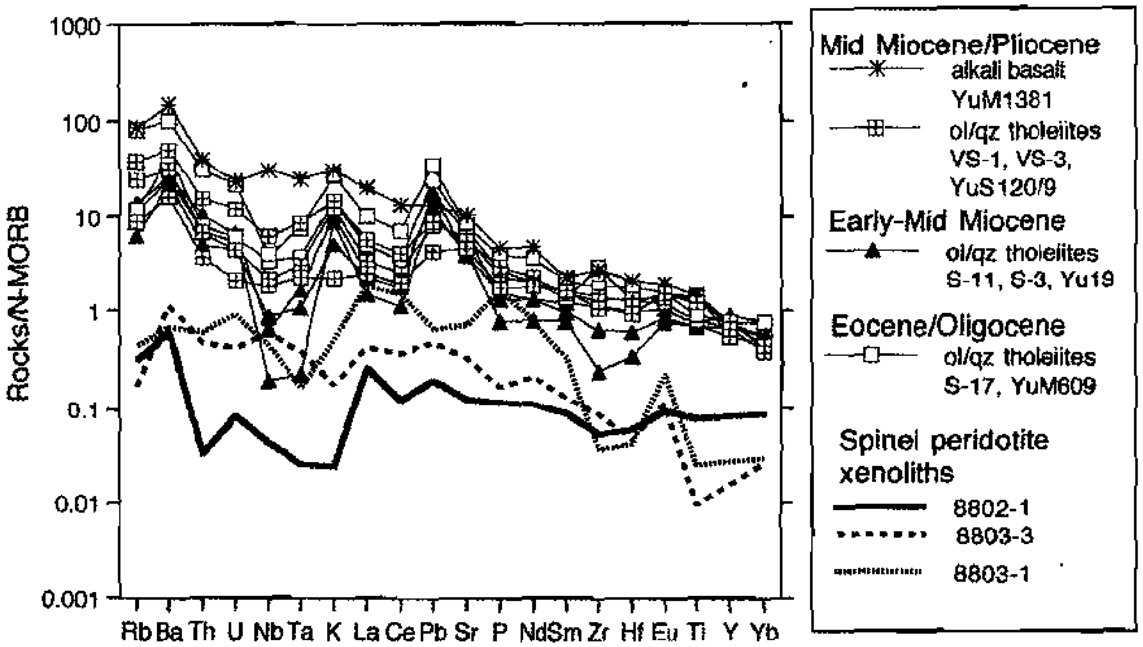

Fig. 6. N-MORB-normalized incompatible element diagrams for selected samples from the Sikhote-Alin and Sakhalin region. Bold lines representing spinel lherzolite xenoliths from Sikhote-Alin (Ionov et al., 1995) are plotted for comparison.

$Zr/Nb > 38$ and $Zr/Y \sim 4$. This range of values falls within those of MORB (Sun & McDonough, 1989). It is clear, however, that the Eocene–Oligocene basalts and some Mid-Miocene–Pliocene basalts lie off the mixing hyperbola.

Compatible trace elements such as Ni and Cr vary widely in concentration. Both are high in the Mid-Miocene–Pliocene basalts, up to 190 and 350 ppm, respectively, and, within this group, both elements show a strong correlation with MgO (Fig. 10b and c). These features are consistent with fractional crystallization of both olivine and pyroxene, and also chrome spinel. There is a crude positive correlation between MgO and Sc for the Mid-Miocene–Pliocene and Eocene–Oligocene lavas, suggesting that pyroxene fractionation may contribute to the Cr variation in addition to Cr-spinel. The Early–Mid-Miocene lavas have high Sc contents (Fig. 10a) and pyroxene fractionation seems to be precluded as an explanation for their low Cr contents. Compared with the Mid-Miocene–Pliocene quartz tholeiites with similar MgO contents, the Mid-Miocene–Pliocene alkali basalts have lower Ni and Cr contents (Fig. 11), approaching those of the Mudanjian alkali basalts south-west of Sikhote-Alin. The most primitive Mid-Miocene–Pliocene lavas contain 7–9 wt % MgO, but most are not sufficiently Mg-rich to be in equilibrium with Fo_{90} mantle olivine. Thus, they are unlikely to represent primary mantle melts but have undergone small amounts of olivine fractionation, probably <5%, based on whole-rock Ni concentrations >150 ppm in the primitive magmas compared with >235 ppm in primary mantle-derived melts (Sato, 1977). The Mid-Miocene–Pliocene basalts lie below the model melting curves in Fig. 11b, calculated for low (1%) and high (20%) degrees of melting according to the model proposed by Hart & Davis (1978). These characteristics are more consistent with 5–15% olivine fractionation, as shown by the model fractionation trends calculated for the removal of olivine from the MgO-rich primary magmas. In Fig. 11b, we note that primary melts of low MgO content will have relatively low Ni contents. Hart & Davis (1978) suggested that MgO contents for parental liquids from natural basaltic series range from 6 to 13 wt %, and that hydrous partial melting of peridotite leads to magmas with high SiO_2 and low MgO contents, resulting in high D_{Ni} and low primary Ni contents. These calculations suggest that the most magnesian alkali basalts may have experienced >5% olivine fractionation from a primary melt with more than 10 wt % MgO, whereas the quartz tholeiites could have experienced only 1–2 wt % olivine fractionation from a melt with less than 7 wt % MgO. The Eocene–Oligocene and Early–Mid-Miocene basalts, characterized by lower Ni and Cr contents (Fig. 10b and c), are clearly not primary melts (in the sense of being in equilibrium with a Fo_{90}–En_{90} dominated upper mantle) and must have undergone considerable olivine fractionation.

Sr–Nd–Pb isotopic compositions

The Sikhote-Alin and Sakhalin samples exhibit a significant range of $^{87}Sr/^{86}Sr$ and $^{143}Nd/^{144}Nd$ (Fig. 12). Two broad groups can be distinguished: (1) a trend of increasing $^{87}Sr/^{86}Sr$ with decreasing $^{143}Nd/^{144}Nd$, seen

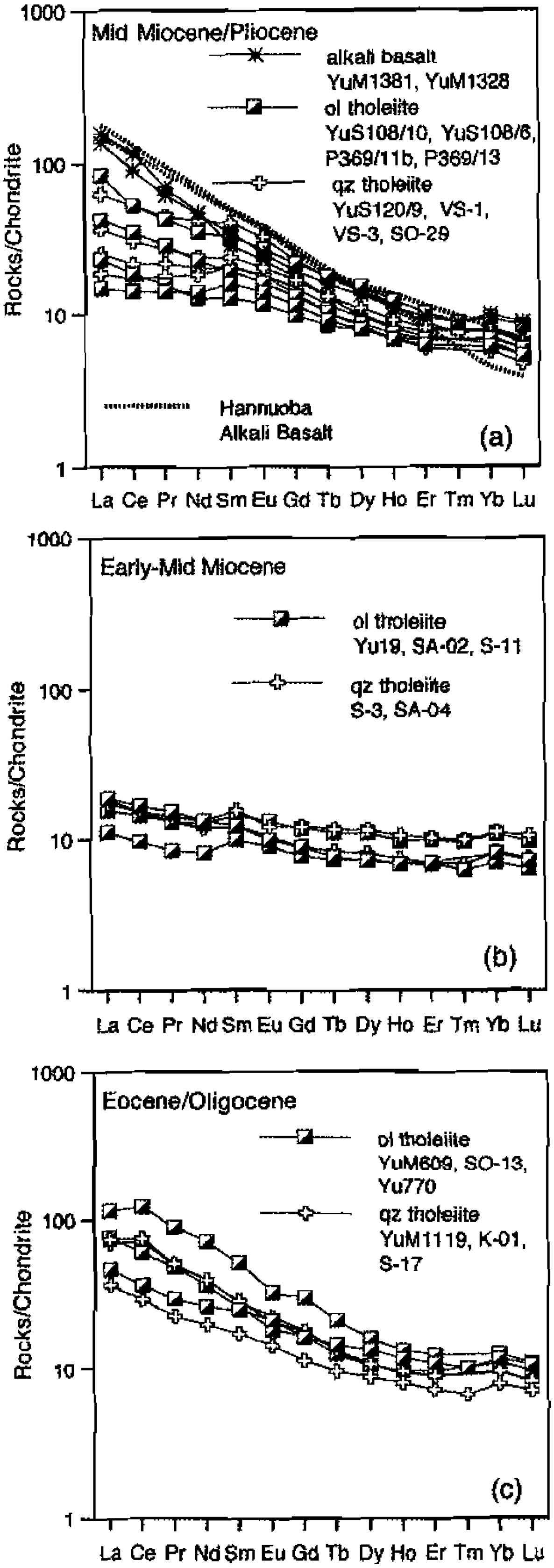

Fig. 7. Chondrite-normalized REE patterns for: (a) Mid-Miocene–Pliocene basalts; (b) Early–Mid-Miocene basalts; (c) Eocene–Oligocene basalts. Representative Hannuoba alkali basalts (Zhu *et al.*, 1990) are also plotted. Normalizing values from Sun & McDonough (1989).

predominantly in the Eocene–Oligocene lavas; (2) a scatter in both Nd- and Sr-isotope composition for the Mid-Miocene–Pliocene lavas. The Eocene–Oligocene basalts have variable $^{87}Sr/^{86}Sr$ (0·7036–0·7051) and $^{143}Nd/^{144}Nd$ (0·51265–0·51290), and are similar isotopically to north-east Honshu Japanese arc lavas. The Early Mid-Miocene basalts have a more restricted range of $^{87}Sr/^{86}Sr$ (0·7033–0·7036) and $^{143}Nd/^{144}Nd$ (0·51288–0·51292), and are the most unradiogenic in $^{87}Sr/^{86}Sr$ and radiogenic in $^{143}Nd/^{144}Nd$ of the Sikhote-Alin and Sakhalin rocks. Within the Mid-Miocene–Pliocene basalts, the lavas of south Sikhote-Alin have relatively high $^{87}Sr/^{86}Sr$ and low $^{143}Nd/^{144}Nd$ similar to the Eocene–Oligocene lavas, whereas those of central Sikhote-Alin have significantly lower-&QJ;$^{143}Nd/^{144}Nd$ and $^{87}Sr/^{86}Sr$ extending toward the enriched mantle end-member EMI (Hofmann, 1997) or a lower-crustal component (Zartman & Haines, 1988).

The lead isotope ratios for all of the Sikhote-Alin and Sakhalin samples plot above the Northern Hemisphere Reference Line (NHRL; as defined by the Pacific MORB array), with elevated $^{207}Pb/^{204}Pb$ and $^{208}Pb/^{204}Pb$ compared with typical MORB and OIB, over a large range in $^{206}Pb/^{204}Pb$ (Fig. 13a and b). The $^{208}Pb/^{204}Pb$ at a given $^{206}Pb/^{204}Pb$ is higher in the Mid-Miocene–Pliocene lavas than in the Eocene–Oligocene and Early–Mid-Miocene lavas. The $^{206}Pb/^{204}Pb$ for the Mid-Miocene–Pliocene samples ranges from 17·26 to 18·32 for the tholeiites (Table 3). The Mid-Miocene–Pliocene tholeiites also trend to the low $^{206}Pb/^{204}Pb$, low $^{207}Pb/^{204}Pb$ end of the NHRL, and plot on the left side of the 4·55 Ga geochron, similar to the Parana flood basalts of Brazil (Hawkesworth *et al.*, 1986), Indian MORB (Mahoney *et al.*, 1989, 1992), and basalts from eastern China (Song *et al.*, 1990; Zhang *et al.*, 1998). Low $^{206}Pb/^{204}Pb$ ratios may indicate a significant role for the continental lithosphere in basalt petrogenesis as an ancient (>10^9 year), isolated mantle reservoir (e.g. Michard *et al.*, 1986; Price *et al.*, 1986). Four distinct source components involved in the petrogenesis of the Sikhote-Alin and Sakhalin samples may be identified on the basis of Figs 13 and 14. Most of the isotope compositions of the Eocene–Oligocene and Early–Mid-Miocene basalts define an array consistent with mixing of two geochemically distinct components—DMM (depleted MORB-source mantle) and EMII (enriched-mantle type II). In contrast, the Mid-Miocene–Pliocene basalts define a distinctly different array. The Mid-Miocene–Pliocene tholeiites have high $^{87}Sr/^{86}Sr$, $^{207}Pb/^{204}Pb$ and $^{208}Pb/^{204}Pb$ and low $^{143}Nd/^{144}Nd$ and $^{206}Pb/^{204}Pb$ isotopic signatures that

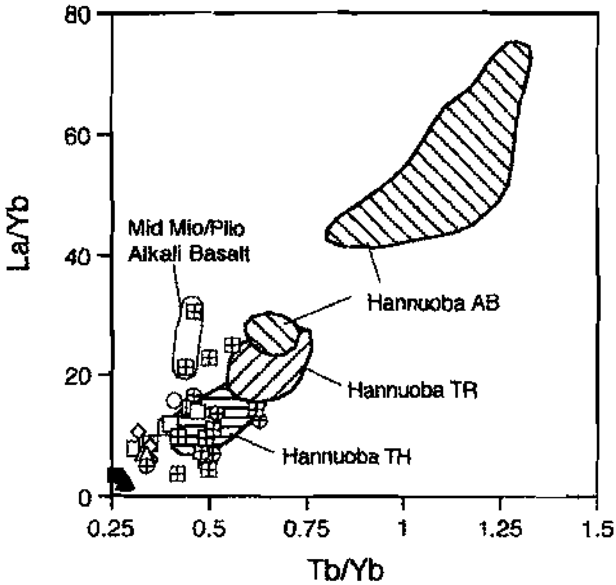

Fig. 8. La/Yb vs Tb/Yb for Sikhote-Alin–Sakhalin volcanic rocks. Fields for Hannuoba basalts (AB, alkali basalt; TR, transitional basalt; TH, tholeiite) from Zhi *et al.* (1990). Symbols as in Fig. 3.

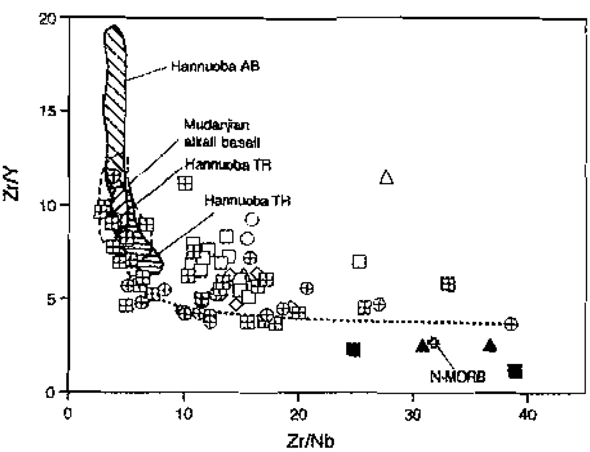

Fig. 9. Zr/Y vs Zr/Nb for Sikhote-Alin–Sakhalin volcanic rocks and Mudanjian alkali basalts. Dotted line is mixing hyperbola calculated between the two extreme points of the dataset, using the equations of Langmuir *et al.* (1978). N-MORB composition (open cross) from Sun & McDonough (1989). Hannuoba alkali basalts as in Fig. 8. Symbols as in Fig. 3.

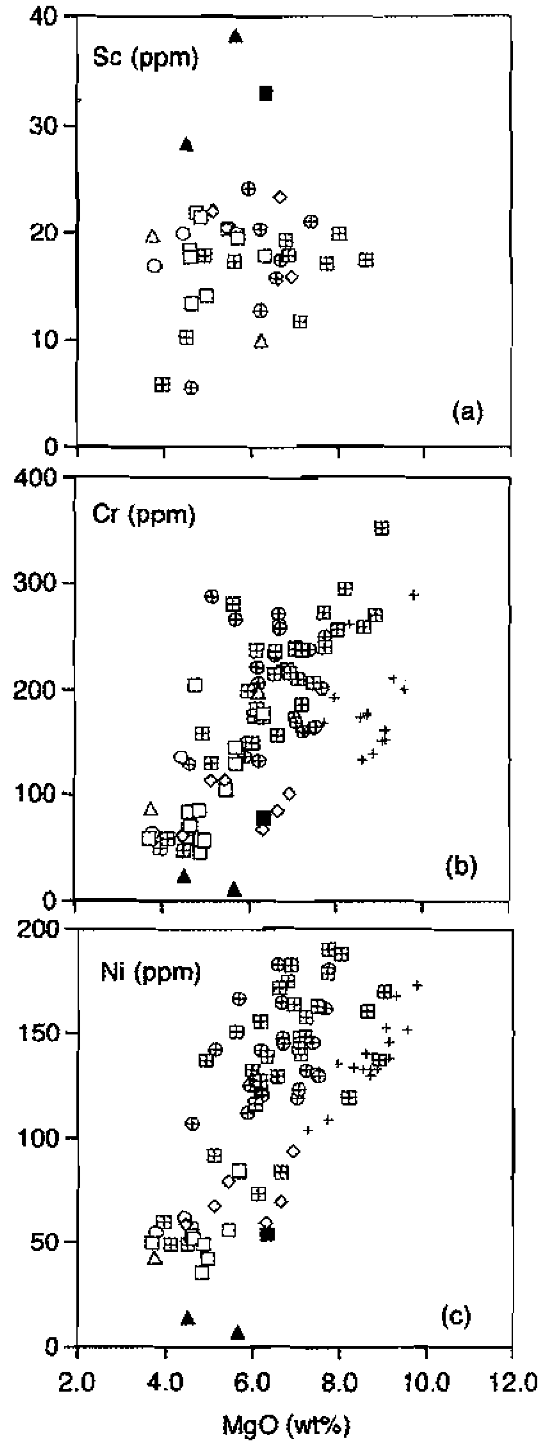

Fig. 10. Wt % MgO vs (a) Sc, (b) Cr and (c) Ni for Sikhote-Alin Sakhalin volcanic rocks and Mudanjian alkali basalts. Symbols as in Fig. 3.

are well outside the range of oceanic basalts, but the closest in composition to the hypothetical end-member EMI or lower crust.

DISCUSSION

Crustal assimilation vs enriched lithosphere

Based on incompatible-element abundances, particularly the depletions in Nb and Ta relative to elements of similar incompatibility in upper-mantle melting processes, it is evident that the petrogenesis of the Eocene–Oligocene basalts and some Mid-Miocene-Pliocene tholeiites differs from that of oceanic island

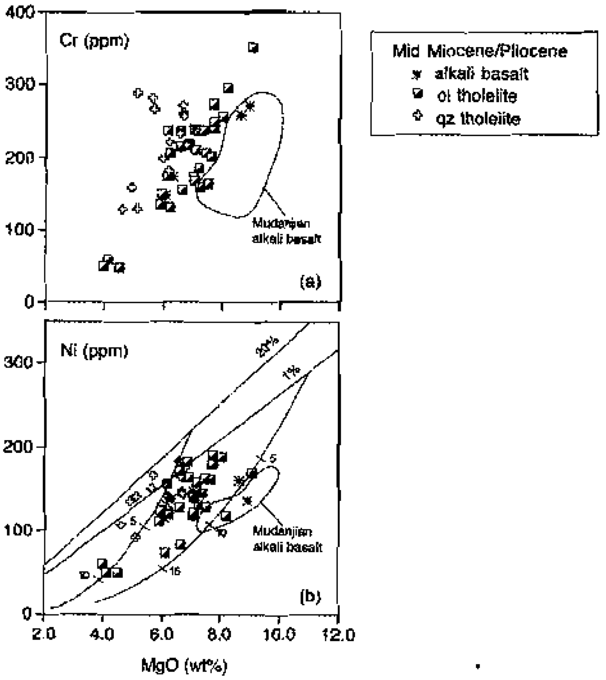

Fig. 11. Wt % MgO vs (a) Cr and (b) Ni for Mid-Miocene–Pliocene basalts from Sikhote-Alin. Partial melting curves are for 1 and 20% batch partial melts of spinel lherzolite. The Ni contents of partial melts of various MgO have been calculated using the Ni partition relationship given by Hart & Davis (1978): D_{Ni} (Ni in olivine/Ni in liquid) = (124/MgO) − 0·9. The initial modal mineralogy, the melting proportions and mineral–mineral partition coefficients for Ni are used following the procedure of Hart & Davis (1978). Fractional crystallization curves are shown for liquids starting on the 1 and 20% melting lines with MgO contents of 11 and 7%, respectively. Numbers at cross-ticks are the amount of olivine crystallized. Olivine fractionation calculated assuming variation of D_{Ni} with MgO given by Hart & Davis (1978).

tholeiites, and is perhaps more similar to that of continental flood basalts, such as the Columbia River (USA) and Karoo (southern Africa) (Wright *et al.*, 1989; Hooper & Hawkesworth, 1993; Lassiter & DePaolo, 1997). Many continental flood basalts have pronounced depletions in HFSE relative to within-plate basalts from oceanic settings, as indicated, for example, by low Nb/La (Arndt & Christensen, 1992). Average continental crust is also strongly depleted in HFSE (Taylor & McLennan, 1985). These observations have led many researchers to conclude that the low Nb/La characteristics of many continental flood basalt suites require crustal assimilation rather than assimilation of continental lithospheric mantle (Arndt *et al.*, 1993; Brandon and Goles, 1995). If the Ta depletion in most Sikhote-Alin and Sakhalin basalts is taken as evidence for crustal assimilation, we would expect a positive correlation between La/Ta and La/Sm, because upper continental crust or moderate-degree partial melts of the lower continental crust will, in general, be enriched in LREE (Taylor & McLennan, 1985). Figure 15 shows La/Sm–La/Ta variations for lavas of

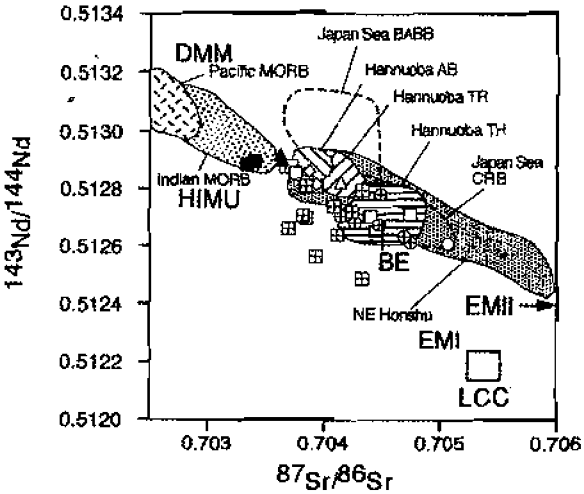

Fig. 12. $^{143}Nd/^{144}Nd$ vs $^{87}Sr/^{86}Sr$ for Sikhote-Alin–Sakhalin volcanic rocks. DMM, depleted MORB-type mantle; HIMU, high-μ-type mantle ($\mu = {}^{238}U/{}^{204}Pb$); EMI and EMII, enriched-mantle type I and type II (Zindler & Hart, 1986; Hart, 1988); LCC, lower continental crust (Zartman & Haines, 1988); BE, Bulk Earth. Data from Hannuoba (Song *et al.*, 1990), north-east Honshu (Kersting *et al.*, 1996) and Pacific and Indian MORB (Hickey-Vargas, 1991) are shown for comparison. Japan Sea BABB and Japan Sea CRB as in Fig. 5. Symbols as in Fig. 3.

the Sikhote-Alin and Sakhalin region. Some lavas do possess relatively high La/Sm and La/Ta values consistent with crustal assimilation. In particular, the Eocene–Oligocene basalts from north and south Sikhote-Alin have elevated La/Sm and La/Ta. However, the Mid-Miocene–Pliocene lavas have variable La/Sm but low La/Ta, and therefore do not appear affected by assimilation of continental crust. The Mid-Miocene–Pliocene alkali basalts have high La/Sm and very low La/Ta similar to those of the East Asian continental alkali basalts, such as Hannuoba. Significantly, the very high La/Ta of the Early–Mid-Miocene basalts, combined with low and constant La/Sm, suggest that the basalts have not experienced significant crustal contamination, but instead were derived from a HFSE-depleted MORB-source mantle component. Lavas with higher La/Sm, which probably have assimilated crustal material, are restricted to some Eocene–Oligocene basalts.

There are two principal hypotheses that can explain the Sr–Nd–Pb isotopic and trace-element characteristics of the Mid-Miocene–Pliocene basalts. They may represent (1) mixing between asthenosphere-derived melts (e.g. alkali basalt) and partial melts of metasomatically enriched, ancient lithospheric mantle, or (2) mixing between asthenosphere-derived melts and partial melts of continental crust or the products of AFC processes. It is clear from the above discussion that some Eocene–Oligocene quartz tholeiites that display positive covariation of La/Sm and La/Ta may have experienced relatively minor crustal contamination. Some workers

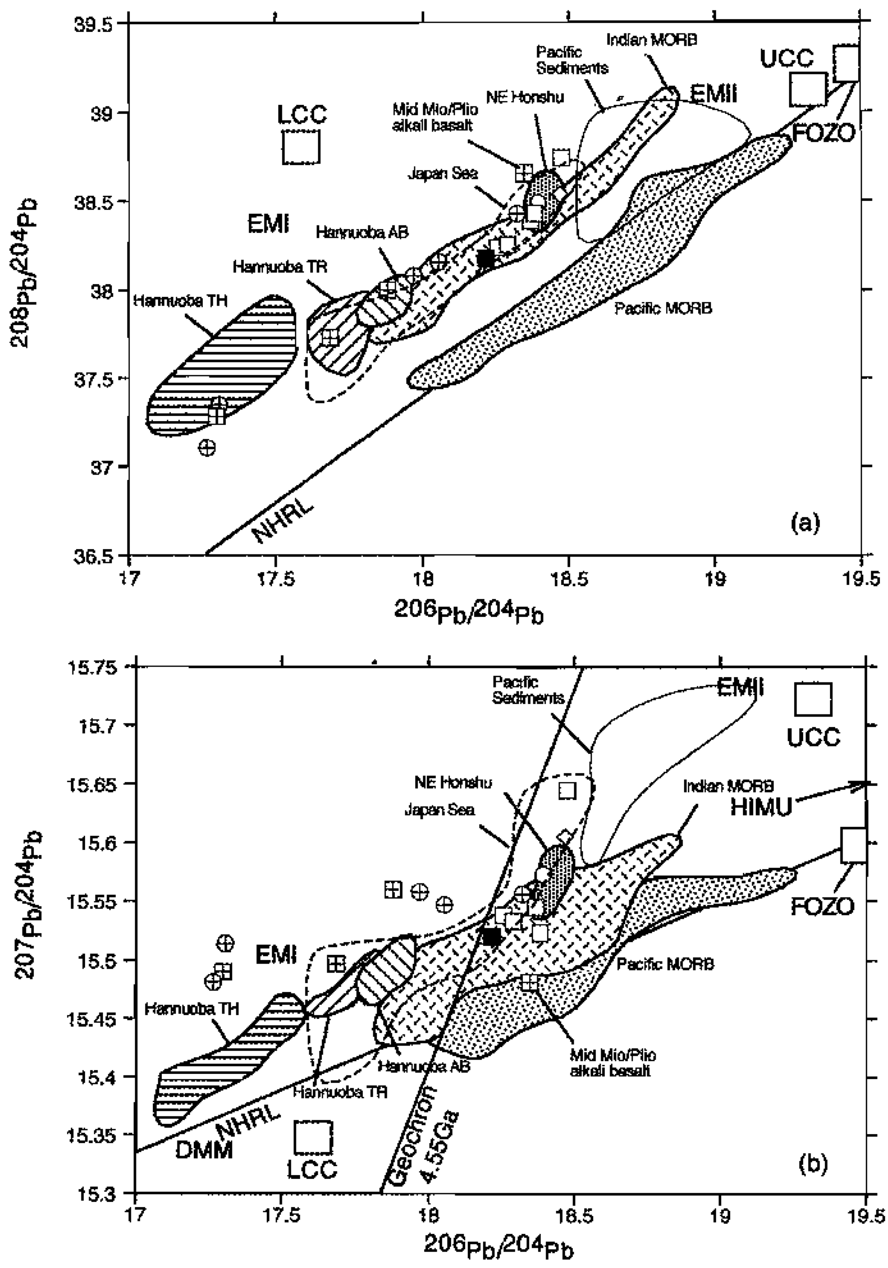

Fig. 13. (a) $^{206}Pb/^{204}Pb$ vs $^{208}Pb/^{204}Pb$ and (b) $^{207}Pb/^{204}Pb$ for Sikhote-Alin–Sakhalin volcanic rocks. UCC, upper continental crust (Zartman & Haines, 1988); FOZO, focal zone (Hart *et al.*, 1992; Hauri *et al.*, 1994); NHRL, Northern Hemisphere reference line (Hart, 1984). Field for Pacific sediments (Cousens *et al.*, 1994) is shown for comparison. Symbols and data sources as in Figs 3 and 12.

have attempted to explain the HFSE depletion in continental flood basalts by the contamination of OIB-like magmas with continental crust (e.g. Thompson *et al.*, 1983). Ormerod *et al.* (1988) argued that the low Nb contents of the US Basin and Range lavas (10–20 ppm) could not be generated by any crustal contamination scheme involving an OIB-type (asthenospheric) parental magma (~50 ppm Nb) as something of the order of 150–400% crustal material would have to be assimilated. Similarly, to reduce the concentration of Nb in the Mid-Miocene–Pliocene OIB-type alkali basalts from a range of 40–70 ppm to the 4–20 ppm range characteristic of the Mid-Miocene–Pliocene quartz tholeiitic basalts would require the addition of large amounts of crustal material, assuming the latter was entirely devoid of Nb. The compatible trace-elements systematics (Fig. 11) suggest that the most magnesian Mid-Miocene–Pliocene alkali basalts have experienced >5% olivine fractionation from a

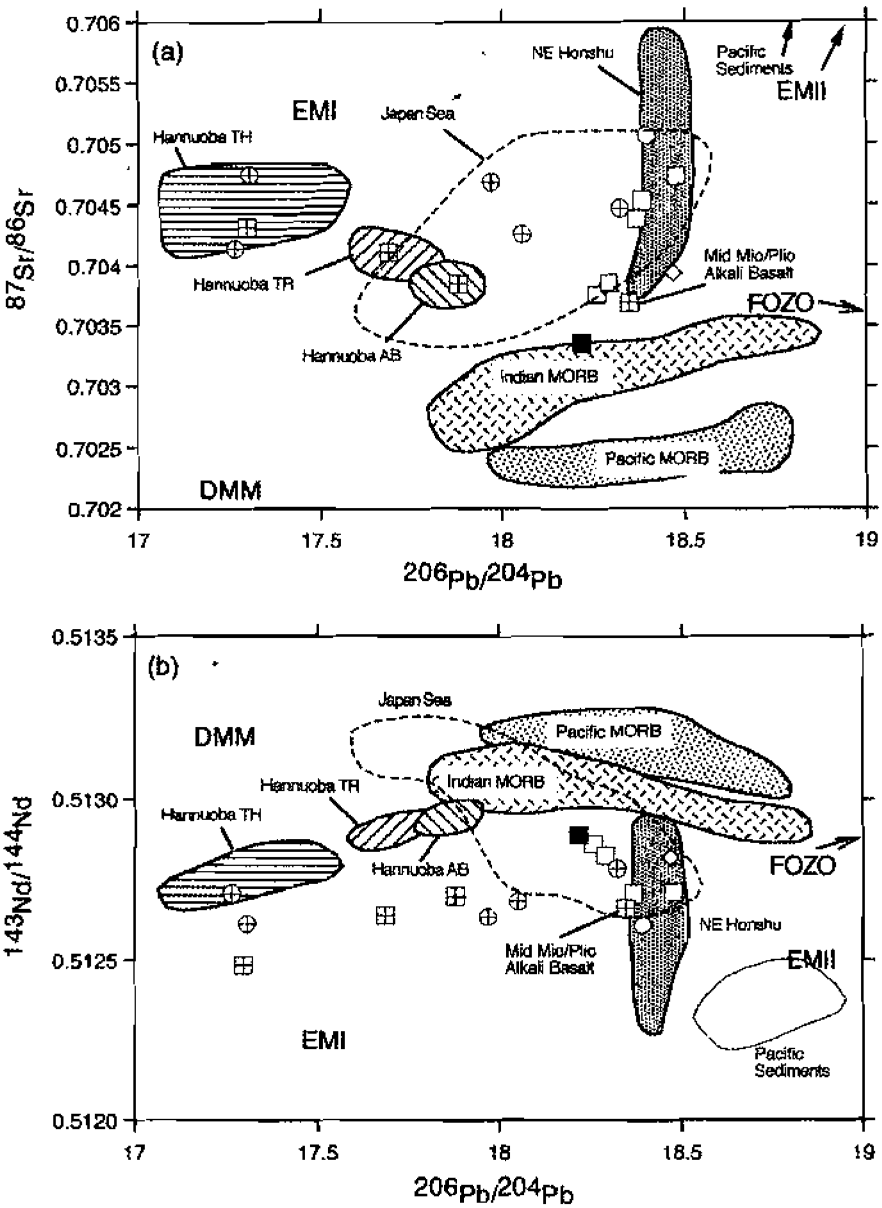

Fig. 14. (a) $^{206}Pb/^{204}Pb$ vs $^{87}Sr/^{86}Sr$ and (b) $^{143}Nd/^{144}Nd$ for Sikhote-Alin–Sakhalin volcanic rocks. Symbols and data sources as in Figs 3, 12 and 13.

primary melt and the quartz tholeiites only 1–2% olivine fractionation. The Mid-Miocene–Pliocene basalts could, therefore, be relatively unmodified mantle melts. Thus, the relative depletions in HFSE cannot result from crustal contamination, but rather reflect the original composition of the mantle source region. The currently available data, therefore, suggest that mixing between mantle-derived alkali basalts and partial melts of continental crust (or AFC) cannot explain all the Sr–Nd–Pb isotopic and trace-element characteristics of the Mid-Miocene–Pliocene tholeiites from the Sikhote-Alin and Sakhalin region.

Identification of source components

Significantly, the higher Ba/Nb and Rb/Nb in the Eocene–Oligocene basalts are characteristics that have typically been associated with subduction-related magmas (Pearce, 1983). These similarities suggest that subduction processes have played some role in the petrogenesis of the Eocene–Oligocene basalts. Fluids driven off a subducting slab inherit their elemental and isotopic characteristics from the subducted oceanic crust, including pelagic sediment, and could, therefore, be very similar to those inferred to have affected the lithospheric

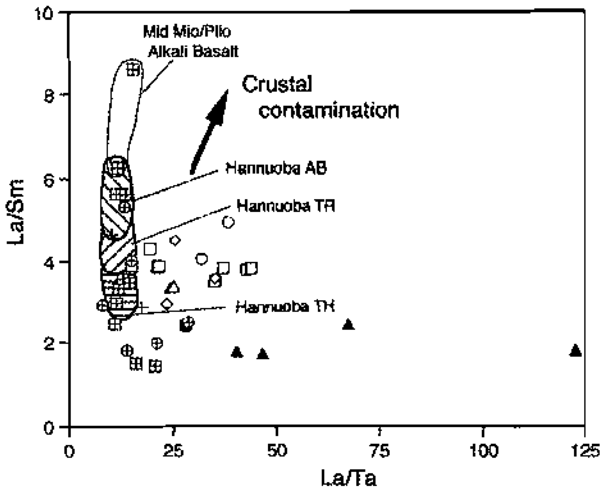

Fig. 15. La/Sm vs La/Ta for the volcanic rocks of the Sikhote-Alin–Sakhalin, the Mudanjian and Hannuoba basalts (Zhi *et al.*, 1990). Symbols and data sources as in Figs 3 and 8.

mantle beneath the Sikhote-Alin and Sakhalin region. These fluids will infiltrate and metasomatize the overlying mantle wedge, which may eventually become accreted to the subcontinental mantle, just as island arc material eventually becomes accreted to the continental crust (Othman *et al.*, 1989).

Most of the Sr–Nd–Pb-isotope compositions of the Eocene–Oligocene and Early–Mid-Miocene basalts erupted pre- and syn-opening of the Sea of Japan define an array consistent with mixing of two geochemically distinct mantle components—EMII and DMM. The Eocene–Oligocene basalts and Early–Mid-Miocene basalts from central Sikhote-Alin and Sakhalin, respectively, exhibit positive correlations between La/Yb and $^{87}Sr/^{86}Sr$ (Fig. 16a). This observation, together with the Nd-isotope data, is consistent with involvement of an incompatible-element-depleted component with a trace-element signature similar to MORB-source mantle (low La/Yb, $^{87}Sr/^{86}Sr$ and high $^{143}Nd/^{144}Nd$). $^{87}Sr/^{86}Sr$

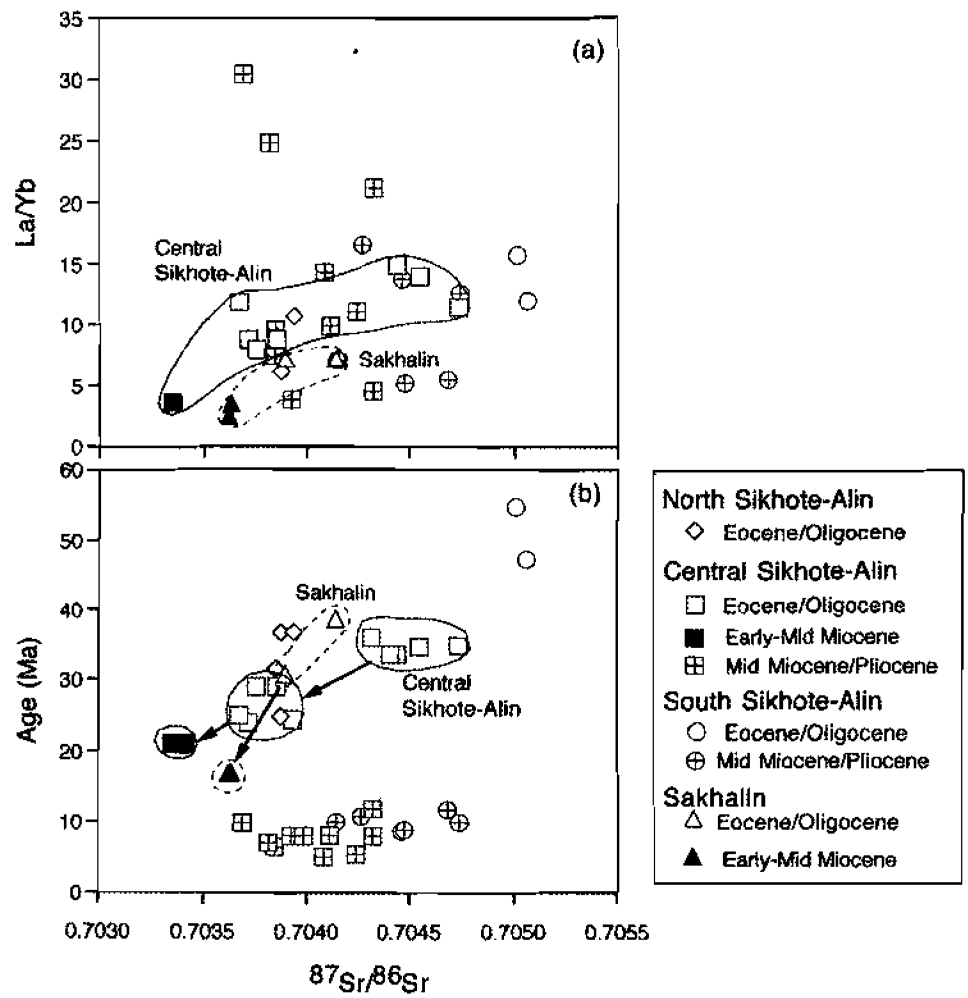

Fig. 16. (a) La/Yb and (b) age vs $^{87}Sr/^{86}Sr$ for the volcanic rocks from Sikhote-Alin–Sakhalin. Symbols as in Fig. 3. Age data from K–Ar dating (Okamura *et al.*, 1998*b*).

ratios of both central Sikhote-Alin and Sakhalin basalts decrease with decreasing age of eruption of the basalts (Fig. 16b). We suggest on this basis that the sites of magma generation beneath Sikhote-Alin and Sakhalin moved down from the subduction-modified, EMII-like mantle lithosphere to the MORB-source asthenosphere as spreading progressed in the Sea of Japan. Paleomagnetic studies indicate that eastward migration of the Japan arc away from eastern Sikhote-Alin has produced the Japan and Yamato Basins (Otofuji & Matsuda, 1984; Otofuji *et al.*, 1994). Continental rifting and the opening of an oceanic basin require flow of asthenosphere into a region previously occupied by subcontinental lithosphere. The source region for the Early–Mid-Miocene basalts erupted during the opening of the Sea of Japan is similar to that of Indian Ocean MORB, i.e. with higher $^{208}Pb/^{204}Pb$ and $^{207}Pb/^{204}Pb$ ratios at a given $^{206}Pb/^{204}Pb$ value than the NHRL (Fig. 13). We suggest that asthenosphere of Indian Ocean MORB source type composes at least part of the Sikhote-Alin–Sakhalin mantle wedge and that there is no contribution of asthenosphere of Pacific Ocean MORB-source mantle to the Cenozoic volcanism of the north-eastern Eurasian margin. Asthenospheric mantle of Indian Ocean MORB-source type, therefore, must have upwelled from beneath the zone of rifting and migrated laterally as the back-arc basin developed between eastern Sikhote-Alin and the Japan arc.

The Sea of Japan basement comprises continental rift tholeiites and back-arc basin basalts erupted during opening in the Early Miocene (Pouclet *et al.*, 1995). Geochemically, the former basalts are mildly LREE-enriched tholeiites with slight Nb depletion, characterized by high $^{87}Sr/^{86}Sr$ and low $^{143}Nd/^{144}Nd$, resembling the Eocene Oligocene basalts (Figs 5 and 12). The latter back-arc basin basalts have neither enrichment nor depletion of LILE, and nearly flat REE patterns intermediate between those of island arc tholeiites and MORB (Fig. 5c). The back-arc basin basalts are the closest in isotopic composition to depleted MORB with low $^{87}Sr/^{86}Sr$ and high $^{143}Nd/^{144}Nd$, similar to those of the Early–Mid-Miocene basalts (Fig. 12). Pouclet *et al.* (1995) proposed that during opening of the Sea of Japan, the mantle source regions involved in magma genesis were (asthenospheric) depleted mantle forming back-arc basin basalts, and subcontinental lithosphere of EMII-like composition (forming continental rift tholeiites), strongly contaminated by subduction-related components.

The Early–Mid-Miocene basalts are distinctive because they have generally lower trace-element concentrations than any other Sikhote-Alin and Sakhalin basalts. The most striking geochemical feature is the relatively low abundance of the HFSE with respect to the LILE—a geochemical feature commonly found in island-arc volcanics (Gill, 1981). The Early–Mid-Miocene basalts are also depleted in HFSE, Y and HREE relative to the back-arc basin basalts from the Sea of Japan basement (Fig. 5c), and they appear to have been derived from mantle sources that are more depleted in incompatible elements than those tapped during formation of the Sea of Japan back-arc basin basalts. Source depletion by melt extraction, prior to arc magma genesis, explains the similar degree of Y depletion and, by analogy, the HREE depletion, to that of HFSE in island arc basalts (Woodhead *et al.*, 1993). Pearce & Parkinson (1993) and Woodhead *et al.* (1993) argued that island arc basalts can be produced by melting of depleted, residual mantle sources after prior back-arc basin basalt melt extraction. The Early–Mid-Miocene basalts are characterized by higher LILE relative to MORB, but low absolute concentrations of Nb, Ta, Zr and Hf, requiring a petrogenesis involving re-fertilization (metasomatism) of a depleted mantle source to create a LILE-enriched source. An appropriate working petrogenetic model is that the Early–Mid-Miocene basalts were derived from a depleted residual asthenospheric mantle source after the back-arc basin basalts had been extracted, closely associated with an influx of LILE-enriched but HFSE-depleted subduction-related melts or fluids. The marked porphyritic character of the Early–Mid-Miocene basalts, compared with other Sikhote-Alin and Sakhalin suites, is documented in Table 1. It is noteworthy that although the overall phenocryst assemblage is the same in the Early–Mid-Miocene as in the other Sikhote-Alin and Sakhalin lavas, some plagioclase core compositions are strikingly anorthitic, consistent with higher water contents in the magmas (Arculus & Wills, 1980). Higher water contents and lower eruption temperatures may have been factors leading to a greater degree of crystallinity of the Early–Mid-Miocene basalts.

The decoupling of trace-element and Sr–Nd–Pb-isotopic ratios in the Sikhote-Alin and Sakhalin lavas, and their contrast with the trace-element patterns characteristic of OIB, suggest that local mantle source enrichment processes, operating over varying time-scales, have played a role in the petrogenesis of the magmas. The relatively minor Mid-Miocene–Pliocene alkali basalts were erupted during the late stage of the lava sequences. The normalized trace-element abundance patterns of the Mid-Miocene–Pliocene alkali basalts are more similar to those of Hawaiian alkali basalts, which are generally considered to be plume-related. OIB are thought to be the products of partial melting of several components within the mantle (Zindler & Hart, 1986), one of which (EMI) may be recycled continental lithospheric mantle (McKenzie & O'Nions, 1983). This clearly complicates the recognition of lithospheric mantle signatures. However, OIB undoubtedly represent magmas mostly generated within the asthenosphere, with or without source component additions from mantle plumes. The trace-element characteristics of the uncontaminated Mid-Miocene–Pliocene alkali basalts are similar to those of the Hannuoba alkali basalts (Figs 9 and 15), consistent with melting of asthenospheric mantle at depth (Song *et al.*, 1990). Barry & Kent (1998) claimed that OIB-like Cenozoic basalts have been erupted in eastern China, Mongolia and Siberia since at least 30 Ma, concurrent with subduction-related active continental-margin volcanism in the Eocene–Oligocene within the Sikhote-Alin and Sakhalin region. The OIB and MORB data arrays in Sr–Nd–Pb-isotope space trend toward a focal zone (FOZO in Figs 13 and 14) between DMM and HIMU; FOZO might be a component from the lower mantle (Hart *et al.*, 1992) or the Transitional Zone (Hanan & Graham, 1996). On the basis of their isotope systematics, the Mid-Miocene–Pliocene alkali basalts may have been derived from an OIB-type mantle source mixed with a FOZO-like component.

We can be confident that deviations from intraoceanic OIB compositions must represent input from additional sources. The Mid-Miocene–Pliocene tholeiitic magmas are characterized by low $^{206}Pb/^{204}Pb$ coupled with high $^{207}Pb/^{204}Pb$ and $^{208}Pb/^{204}Pb$—features typical of the EMI mantle end-member (Hofmann, 1997) (Fig. 13). These characteristics were originally referred to as the DUPAL anomaly—a circumglobal anomaly related to a temporally persistent mantle convection system centered on latitude 30°S (Hart, 1984). The distribution of Dupal-type oceanic basalts within the Southern Hemisphere was linked to a sublithospheric mantle reservoir, either derived from mantle plumes involving significant amounts of ancient subducted sediments (Hart, 1988; Castillo, 1988) or thermally eroded Gondwana lithospheric mantle (Hawkesworth *et al.*, 1986). For example, ancient continental lithosphere with a Dupal signature was considered to be dispersed and incorporated into the Indian Ocean MORB source during the break-up of Gondwana (Mahoney *et al.*, 1989, 1992). Similar Pb-isotope characteristics, and broadly similar Sr- and Nd-isotope compositions, are observed in the nearby, contemporaneous, East Asian basalts, such as the Hannuoba tholeiites (Figs 13 and 14). For Hannuoba, Zhi *et al.* (1990) and Song *et al.* (1990) attributed the DUPAL isotopic characteristics of the tholeiites to melting of ancient subcontinental lithospheric mantle during continental extension, and the distinct characteristics of the alkali basalts either to melting of the lowermost lithosphere or the asthenophere. Thus, by inference, it appears that the low $^{206}Pb/^{204}Pb$ characteristics of the Mid-Miocene–Pliocene tholeiitic magma is likely to be a lithospheric mantle feature.

In summary, we suggest that there is an indication that mixing of mantle sources was an important process in the origin of the Mid-Miocene–Pliocene basalts erupted post opening of the Sea of Japan, with end-members being an enriched OIB-type mantle source similar to FOZO, and an EMI-type mantle source. The Nb and Ta depletions in some of the Mid-Miocene–Pliocene tholeiites (Fig. 5b) are more consistent with a subduction-modified mantle source. We conclude that the Mid-Miocene–Pliocene tholeiitic basalts require a significant contribution from an enriched EMI-type Precambrian subcontinental lithospheric mantle source, in part possibly modified by ancient (>10^9 year) metasomatism above a subduction zone. The Eocene–Oligocene and Early–Mid-Miocene basalts have EMII- and DMM-type signatures and do not show any conclusive geochemical signatures for derivation from FOZO- and EMI-type mantle sources during the pre- and syn-opening phases.

Lateral variation of lithospheric thickness

The Mid-Miocene–Pliocene basalts have lower La/Yb and Tb/Yb ratios than the Hannuoba alkali basalts (Fig. 8). The systematically different La/Yb and similar HREE abundances could have been produced by melting of spinel lherzolite beneath the Sikhote-Alin and Sakhalin region. Because the Hannuoba alkali basalts and the Mid-Miocene–Pliocene alkali basalts are characterized by similar isotopic signatures (e.g. Nd- and Sr-isotope ratios intermediate between those of MORB and inferred for the Bulk Earth), the REE differences between the Hannuoba and the Mid-Miocene–Pliocene basalts (Fig. 8) are to be expected given the tectonic settings of the two provinces. The transition from spinel to garnet lherzolite close to the peridotite solidus probably occurs at pressures in excess of 2·5 GPa (Hirschmann & Stolper, 1996). As these minimum depths of melt separation are correlated with thickening of the lithosphere from the continental margin (Sikhote-Alin and Sakhalin region) to the continental interior (Hannuoba), they may reflect dominantly asthenospheric melting for the intra-plate, OIB-like alkali basalts. The more pronounced garnet signature in the REE patterns of relatively uncontaminated Hannuoba alkali basalts compared with the Mid-Miocene–Pliocene basalts is consistent with the interpretation that the Hannuoba basalts are primarily generated through small degrees of partial melting of hot mantle beneath a thick lithospheric lid.

Abundant spinel lherzolite xenoliths are present in the Mid-Miocene–Pliocene alkali basalts in the Sikhote-Alin region. Ionov *et al.* (1995) reported spinel lherzolites with accessory plagioclase from the Koppy River near the Sovgavan and Nelma Plateaux, which suggests a shallow source region for the xenoliths at a depth of ~50 km, within the transition between the plagioclase lherzolite and spinel lherzolite stability fields. Geophysical data indicate relatively thin crust (~25–30 km) beneath

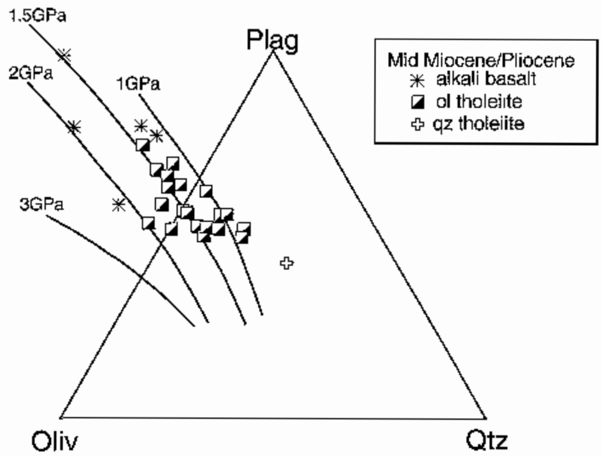

Fig. 17. Composition of estimated primary magma for the Mid-Miocene–Pliocene basalts from Sikhote-Alin–Sakhalin region projected into the pseudoternary system olivine plagioclase–quartz (Olv–Plag–Qtz). Normative components are calculated following expressions given by Grove *et al.* (1992). All components have been normalized to equal oxygen units. The compositions of anhydrous partial melts of peridotite formed at 1–3 GPa (10–30 kbar) (Hirose & Kushiro, 1993) are shown by continuous lines.

eastern Sikhote-Alin (Karp & Lelikov, 1990). Projections of estimated primary basalt (melt plus ~6% of fractionated olivine) compositions for Mid-Miocene–Pliocene basalts from the Sikhote-Alin and Sakhalin region in the pseudoternary system olivine–plagioclase–quartz (Olv–Plag–Qtz), using the procedure of Takahashi (1986), are shown in Fig. 17. One interpretation of the projected data relative to high-pressure cotectics is that primary magma segregation for all primitive basaltic compositions occurred at depths of less than 70 km (~2 GPa or 20 kbar). Therefore, petrological and geophysical evidence is consistent with the existence of a thin lithospheric lid beneath the Sikhote-Alin and Sakhalin region. The basalt-hosted xenoliths from Hannuoba are dominantly spinel lherzolite with subordinate amounts of pyroxenite and garnet lherzolite (Tatsumoto *et al.*, 1992). Fan *et al.* (2000) suggested that seismic, heat flow and thermobarometric data indicate that the present-day lithosphere beneath eastern China is ~80 km thick. The geochemical differences between the Hannuoba alkali basalts and the Mid-Miocene–Pliocene alkali basalts probably represent a lateral variation in lithospheric thickness from eastern China to the Sikhote-Alin and Sakhalin region (Sea of Japan).

The major- and trace-element compositions of the spinel lherzolite xenoliths from Sikhote-Alin provide evidence of depletion and enrichment events and indicate large-scale mantle heterogeneities within accreted lithospheric blocks of different provenance and metasomatism during continental rifting (Ionov *et al.*, 1995). Ionov *et al.* (1995) suggested that the higher oxygen fugacity inferred in the mantle beneath Sikhote-Alin (Ionov & Wood, 1992) relative to inland central Asia may be a regional feature related to the fact that Sikhote-Alin is located close to the continental margin. We propose that the metasomatic event recorded in the thin lithospheric mantle beneath Sikhote-Alin resulted from continental rifting closely related to the opening of the Sea of Japan. Cenozoic basalts and associated mantle xenoliths from eastern China indicate that an EMII mantle domain may be present in the Chinese continental lithosphere just above an EMI domain in the lower part of the lithosphere (Tatsumoto *et al.*, 1992). As the Eocene–Oligocene and Early–Mid-Miocene basalts have EMII- and DMM-type signatures and fail to show any conclusive geochemical signatures for derivation from an EMI-type enriched subcontinental lithospheric mantle during the pre- and syn-opening phases, the mantle lithosphere under Sikhote-Alin and Sakhalin may have preserved only the EMII mantle domain (Fig. 18a and b). The appearance of FOZO- and EMI-type components in the post-opening Mid-Miocene–Pliocene basalts may reflect mantle flow into the region through asthenospheric injection under north-east China that led to thinning of the subcontinental lithosphere via partial delamination. The source of the FOZO-related alkali basalts was most obviously tapped during post-opening magmatism. If we assume that the FOZO-type component was derived from the upwelling asthenosphere beneath north-east China, then it is likely that the Japan Sea opening and associated magmatism in the back-arc basin were triggered by lateral migration of the FOZO-type asthenospheric mantle from beneath north-east China toward the Japan arc (Fig. 18b and c).

CONCLUDING REMARKS

High Ba/Nb and Rb/Nb in the Eocene–Oligocene samples suggest that subduction processes have played a role in the petrogenesis of basalts of this age. The Early–Mid-Miocene basalts are the closest in isotopic composition to depleted MORB, similar to the back-arc basin basalts from the Sea of Japan. On the other hand, these basalts are characterized by higher LILE relative to MORB, but low absolute concentrations of HFSE, Y and HREE relative to the back-arc basin basalts. Thus, the most likely petrogenetic model is that the Early–Mid-Miocene basalts were derived from depleted residual asthenospheric mantle after the back-arc basin basalts were produced, and were closely associated with an influx of highly LILE-enriched and HFSE-depleted melt or fluid related to subduction. The Sr–Nd–Pb isotopic and trace-element systematics of the Eocene–Oligocene basalts and Early–Mid-Miocene basalts suggest that the sites of magma generation beneath the Sikhote-Alin and Sakhalin region have moved from subduction-enriched lithosphere deeper into MORB-type asthenosphere as spreading progressed in the Sea of Japan.

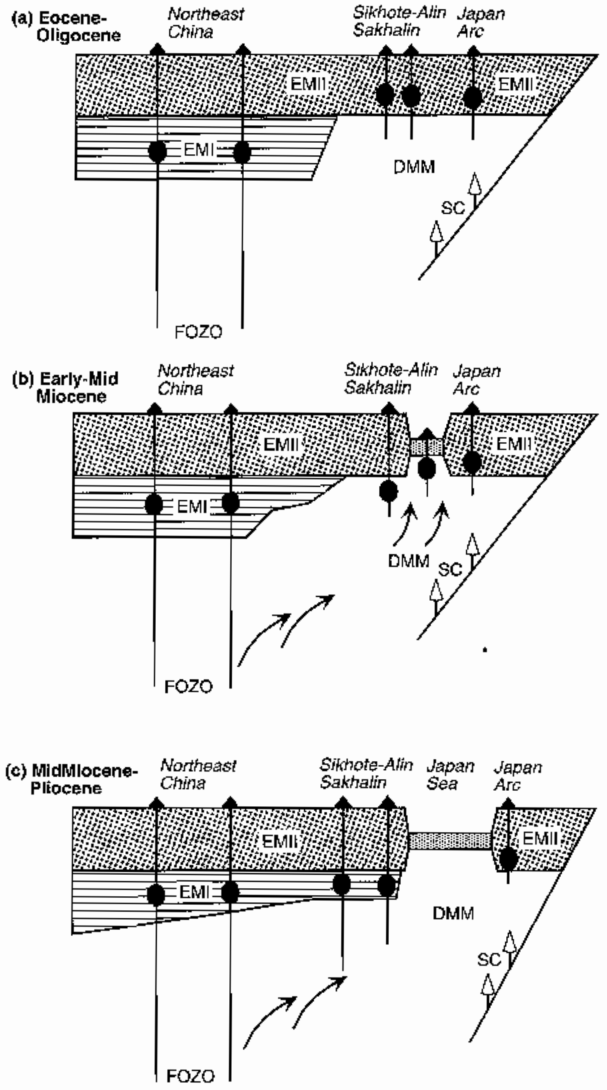

Fig. 18. Schematic cross-section illustrating tectonic model of north-eastern Eurasian margin for (a) pre-opening stage, (b) syn-opening stage and (c) post-opening stage of the Sea of Japan. SC, subduction components.

The post-Sea of Japan opening Mid-Miocene–Pliocene lavas exhibit wide ranges in trace-element abundances that vary between two distinct end-member types. The minor Mid-Miocene–Pliocene alkali basalts have OIB-like trace-element and Sr–Nd–Pb-isotope compositions, similar to the Hannuoba alkali basalts from the East Asian continent, consistent with melting of asthenospheric mantle at depth. By contrast, the Mid-Miocene–Pliocene tholeiites form the other extreme with HFSE concentrations that are much lower than those of elements of similar incompatibility. The relative depletions in HFSE are not a feature of crustal contamination processes, but rather reflect lithospheric mantle source region. The wide range of incompatible-element abundances in the Mid-Miocene–Pliocene basalts defines coherent trends consistent with mantle mixing between an isotopically enriched FOZO-type asthenospheric mantle and an isotopically enriched EMI-type subcontinental lithospheric mantle. The similar isotopic signatures but systematically different REE abundances in the Mid-Miocene–Pliocene alkali basalts and East Asian continental basalts are best modeled by similar extents of melting of spinel lherzolite and garnet lherzolite, respectively. These melting conditions are correlated with thickening of the lithosphere from the continental margin (Sikhote-Alin and Sakhalin region) to the continental interior (East Asian continent). We propose that a heating event closely related to the opening of the Sea of Japan might have resulted in formation of a thin lithospheric lid beneath the Sikhote-Alin and Sakhalin region.

ACKNOWLEDGEMENTS

V. Popov, S. Kovalenko, S. V. Vysotskiy, V. Simanenko, D. F. Semenov and A. Shapotin assisted us in our field studies at Sikhote-Alin and Sakhalin. XRF data were obtained through A. Logan and V. F. Avery. The authors wish to thank J. F. Luhr and T. L. Wright for their comments and improvement of the manuscript. Reviews by anonymous reviewers and the editorial comments by M. Wilson greatly helped to improve this manuscript. Some of the expenses of this research were defrayed by grants from the Australian Research Council. Financial support was provided to S.O. by the Smithsonian Institution Fellowship; both are gratefully acknowledged.

SUPPLEMENTARY DATA

Supplementary data for this paper are available from *Journal of Petrology* online.

REFERENCES

Arculus, R. J. & Wills, K. J. A. (1980). The petrology of plutonic blocks and inclusions from the Lesser Antilles island arc. *Journal of Petrology* 21, 743–799.

Arndt, N. T. & Christensen, U. (1992). The role of lithospheric mantle in continental flood volcanism: thermal and geochemical constraints. *Journal of Geophysical Research* **97**, 10967–10981.

Arndt, N. T., Czamanske, G. K., Wooden, J. L. & Fedorenko, V. A. (1993). Mantle and crustal contributions to continental flood volcanism. *Tectonophysics* **223**, 39–52.

Barry, T. L. & Kent, R. W. (1998). Cenozoic magmatism in Mongolia and the origin of Central and East Asian basalts. In: Flower, M. F. J., Chung, S.-L., Lo, C.-H. & Lee, T.-Y. (eds) *Mantle Dynamics and Plate Interactions in East Asia. American Geophysical Union, Geodynamics Series* **27**, 347–364.

Brandon, A. D. & Goles, G. G. (1995). Assessing subcontinental lithospheric mantle sources for basalts: Neogene volcanism in the Pacific Northwest, USA as a test case. *Contributions to Mineralogy and Petrology* **121**, 364–379.

Castillo, P. (1988). The Dupal anomaly as a trace of the upwelling lower mantle. *Nature* **336**, 667–670.

Cousens, B. L., Allan, J. F. & Gorton, M. P. (1994). Subduction-modified pelagic sediments as the enriched component in back-arc basalts from the Japan Sea: Ocean Drilling Program Sites 797 and 794. *Contributions to Mineralogy and Petrology* **117**, 421–434.

Esin, V., Ponomarchuk, V. A., Shipitsin, Y. G. & Palesskii, S. V. (1995). Petrogenesis of the Sovgavan tholeiite–alkaline basalt plateau in the eastern Sikhote-Alin. *Russian Geology and Geophysics* **36**, 60–68.

Fan, Q. & Hooper, P. R. (1991). The Cenozoic basaltic rocks of eastern China: petrology and chemical composition. *Journal of Petrology* **32**, 765–810.

Fan, W. M., Zhang, H. F., Baker, J., Jarvis, K. E., Mason, P. R. D. & Menzies, M. A. (2000). On and off the North China Craton: where is the Archaean keel? *Journal of Petrology* **41**, 933–950.

Gill, J. B. (1981). *Orogenic Andesites and Plate Tectonics.* Berlin: Springer, pp. 385.

Grove, T. L., Kinzler, R. J. & Bryan, W. B. (1992). Fractionation of mid-ocean ridge basalt (MORB). In: Phipps-Morgan, J., Blackman, D. K. & Sinton, J.M. (eds) *Mantle Flow and Melt Generation at Mid-Ocean Ridges. Geophysical Monograph, American Geophysical Union* **71**, 281–310.

Hanan, B. B. & Graham, D. W. (1996). Lead and helium isotope evidence from oceanic basalts for a common deep source of mantle plumes. *Science* **272**, 991–995.

Hart, S. R. (1984). A large-scale isotope anomaly in the Southern Hemisphere mantle. *Nature* **309**, 753–757.

Hart, S. R. (1988). Heterogeneous mantle domains: signatures, genesis and mixing chronologies. *Earth and Planetary Science Letters* **90**, 273–296.

Hart, S. R. & Davis, K. E. (1978). Nickel partitioning between olivine and silicate melt. *Earth and Planetary Science Letters* **40**, 203–219.

Hart, S. R., Hauri, E. H., Oschmann, L. A. & Whitehead, J. A. (1992). Mantle plumes and entrainment: isotopic evidence. *Science* **256**, 517–520.

Hawkesworth, C. J., Mantovani, M. S. M., Taylor, P. N. & Palacz, Z. (1986). Evidence from the Parana of south Brazil for a continental contribution to Dupal basalts. *Nature* **322**, 356–359.

Hickey-Vargas, R. (1991). Isotope characteristics of submarine lavas from the Philippine Sea: implications for the origin of arc and basin magmas of the Philippine tectonic plate. *Earth and Planetary Science Letters* **107**, 290–304.

Hirose, K. & Kushiro, I. (1993). Partial melting of dry peridotites at high pressures: determination of compositions of melt segregated from peridotite using aggregates of diamond. *Earth and Planetary Science Letters* **114**, 477–489.

Hirschmann, M. M. & Stolper, E. M. (1996). A possible role for garnet pyroxenite in the origin of the 'garnet signature' in MORB. *Contributions to Mineralogy and Petrology* **124**, 185–208.

Hofmann, A. W. (1997). Mantle geochemistry: the message from oceanic volcanism. *Nature* **385**, 219–229.

Hooper, P. R. & Hawkesworth, C. J. (1993). Isotopic and geochemical constraints on the origin and evolution of the Columbia River Basalt. *Journal of Petrology* **34**, 1203–1246.

Ionov, D. A. & Wood, B. J. (1992). The oxidation state of subcontinental mantle: oxygen thermobarometry of mantle xenoliths from central Asia. *Contributions to Mineralogy and Petrology* **111**, 179–193.

Ionov, D. A., Prikhod'ko, V. S. & O'Reilly, S. Y. (1995). Peridotite xenoliths in alkali basalts from the Sikhote-Alin, southeastern Siberia, Russia: trace-element signatures of mantle beneath a convergent continental margin. *Chemical Geology* **120**, 275–294.

Jolivet, L., Shibuya, H. & Fournier, M. (1995). Paleomagnetic rotations and the Japan Sea opening. In: Taylor, B. & Natland, J. (eds) *Active Margins and Marginal Basins of the Western Pacific. Geophysical Monograph, American Geophysical Union* **88**, 355–369.

Kagami, H., Iwata, M., Sano, S. & Honma, H. (1987). Sr and Nd isotopic compositions and Rb, Sr, Sm and Nd concentrations of standard samples. *Technical Report of ISEI Okayama University, Series B* **4**, 16 pp.

Kagami, H., Yokose, H. & Honma, H. (1989). $^{87}Sr/^{86}Sr$ and $^{143}Nd/^{144}Nd$ ratios of GSJ rock reference samples; JB-1a, JA-1 and JG-1a. *Geochemical Journal* **23**, 209–214.

Karp, B. & Lelikov, E. P. (1990). Geological structure, composition and evolution of crustal layers of the Japan Sea. *Tectonophysics* **181**, 277–283.

Kersting, A. B., Arculus, R. J. & Gust, D. A. (1996). Lithospheric contribution to arc magmatism: isotope variations along strike in volcanoes of Honshu, Japan. *Science* **272**, 1464–1468.

Langmuir, C. H., Vocke, R. D., Hanson, G. N. & Hart, S. (1978). A general mixing equation with applications to Icelandic basalts. *Earth and Planetary Science Letters* **37**, 380–392.

Lassiter, J. C. & DePaolo, D. J. (1997). Plume/lithosphere interaction in the generation if continental and oceanic flood basalts: chemical and isotopic constraints. In: Mahoney, J. J. & Coffin, M. F. (eds) *Large Igneous Provinces: Continental, Oceanic, and Planetary Flood Volcanism. Geophysical Monograph, American Geophysical Union* **100**, 335–355.

Le Maitre, R. W., Streckeisen, A., Zanettin, B., Le Bas, M. J., Bonin, B., Bateman, P., *et al.* (eds.) (2002). *Igneous Rocks: a Classification and Glossary of Terms: Recommendations of the International Union of Geological Sciences Subcommission on the Systematics of Igneous Rocks.* Cambridge: Cambridge University Press, 236 pp.

Mahoney, J. J., Natland, J. H., White, W. M., Poreda, R., Bloomer, S. H., Fisher, R. L. *et al.* (1989). Isotopic and geochemical provinces of the western Indian Ocean spreading centers. *Journal of Geophysical Research* **94**, 4033–4052.

Mahoney, J. J., LeRoex, A. P., Peng, Z., Fisher, R. L. & Natland, J. H. (1992). Southwestern limits of Indian Ocean Ridge mantle and the origin of low $^{206}Pb/^{204}Pb$ mid-ocean ridge basalt: isotope systematics of the central Southwestern Indian Ridge (17°–50°E). *Journal of Geophysical Research* **97**, 19771–19790.

McKenzie, D. & O'Nions, R. K. (1983). Mantle reservoirs and ocean island basalts. *Nature* **301**, 229–231.

Michard, A., Montigny, R. & Schlich, R. (1986). Geochemistry of the mantle beneath the Rodriguez triple junction and the South-East Indian Ridge. *Earth and Planetary Science Letters* **78**, 104–114.

Miyashiro, A. (1974). Volcanic rock series in island arcs and active continental margins. *American Journal of Science* **274**, 321–355.

Okamura, S., Arculus, R. J., Martynov, Y. A., Kagami, H., Yoshida, T. & Kawano, Y. (1998*a*). Multiple magma sources involved in marginal-sea formation: Pb, Sr, and Nd isotopic evidence from the Japan Sea region. *Geology* **26**, 619–622.

Okamura, S., Martynov, Y. A., Furuyama, K. & Nagao, K. (1998*b*). K–Ar ages of the basaltic rocks from Far East Russia: constraints on the tectono-magmatism associated with the Japan Sea opening. *The Island Arc* **7**, 271–282.

Ormerod, D. S., Hawkesworth, C. J., Rogers, N. W., Leeman, W. P. & Menzies, M. A. (1988). Tectonic and magmatic transitions in the Western Great Basin, USA. *Nature* **333**, 349–353.

Othman, D. B., White, W. M. & Patchett, J. (1989). The geochemistry of marine sediments, island arc magma genesis, and crust–mantle recycling. *Earth and Planetary Science Letters* **94**, 1–21.

Otofuji, Y. & Matsuda, T. (1984). Timing of rotational motion of southwest Japan inferred from paleomagnetism. *Earth and Planetary Science Letters* **70**, 373–382.

Otofuji, Y., Kambara, A., Matsuda, T. & Nohda, S. (1994). Counter-clockwise rotation of northeast Japan: paleomagnetic evidence for regional extent and timing of rotation. *Earth and Planetary Science Letters* **121**, 503–518.

Pearce, J. A. (1983). Role of the sub-continental lithosphere in magma genesis at active continental margins. In: Hawkesworth, C. J. & Norry, M. J. (eds) *Continental Basalts and Mantle Xenoliths*. Nantwich: Shiva, pp. 230–249.

Pearce, J. A. & Parkinson, I. J. (1993). Trace element models for mantle melting: application to volcanic arc petrogenesis. In: Prichard, H. M., Alabaster, T., Harris, N.B.W. & Neary, C.R. (eds) *Magmatic Processes and Plate Tectonics. Geological Society, London, Special Publications* **76**, 373–403.

Pouclet, A., Lee, J.-S., Vidal, P., Cousens, B. & Bellon, H. (1995). Cretaceous to Cenozoic volcanism in South Korea and in the Sea of Japan: magmatic constraints on the opening of the back-arc basin. In: Smellie, J. L. (ed.) *Volcanism Associated with Extension at Consuming Plate Margins. Geological Society, London, Special Publications* **81**, 169–191.

Price, R. C., Kennedy, A. K., Riggs-Sneeringer, M. & Frey, F. A. (1986). Geochemistry of basalts from the Indian Ocean triple junction: implications for the generation and evolution of Indian Ocean ridge basalts. *Earth and Planetary Science Letters* **78**, 379–396.

Sato, H. (1977). Nickel content of basaltic magmas; identification of primary magma and a measure of the degree of olivine fractionation. *Lithos* **10**, 113–120.

Song, Y., Frey, F. A. & Zhi, X. (1990). Isotopic characteristics of Hannuoba basalts, eastern China: implications for their petrogenesis and the composition of subcontinental mantle. *Chemical Geology* **85**, 35–52.

Sun, S. S. & McDonough, W. F. (1989). Chemical and isotopic systematics of oceanic basalts: implications for mantle composition and processes. In: Saunders, A. D. & Norry, M. J. (eds) *Magmatism in the Ocean Basins. Geological Society, London, Special Publications* **42**, 313–345.

Takahashi, E. (1986). Origin of basaltic magmas. *Bulletin of the Volcanological Society of Japan* **30**, S17–S40 (in Japanese with English abstract).

Tamaki, K., Suyehiro, K., Allan, J., Ingle, C. & Pisciotte, K. A. (1992). Tectonic synthesis and implications of Japan Sea ODP drilling. In: Tamaki, K., Suyehiro, K., Allan, J. & McWilliams, M. (eds) *Proceedings of the Ocean Drilling Program, Scientific Results 127/128*. College Station, TX: Ocean Drilling Program, pp. 1333–1348.

Tatsumi, Y., Sato, K. & Sano, T. (2000). Transition from arc to intraplate magmatism associated with backarc rifting: evolution of the Sikhote Alin volcanism. *Geophysical Research Letters* **27**, 1587–1590.

Tatsumoto, M., Basu, A. R., Wankang, H., Junwen, W. & Guanghong, X. (1992). Sr, Nd, and Pb isotopes of ultramafic xenoliths in volcanic rocks of eastern China: enriched components EMI and EMII in subcontinental lithosphere. *Earth and Planetary Science Letters* **113**, 107–128.

Taylor, S. R. & McLennan, S. M. (1985). *The Continental Crust: Its Composition and Evolution*. London: Blackwell Scientific, 312 pp.

Thompson, R. N. (1984). Dispatches from the basalt front. I. Experiments. *Proceedings of the Geologists' Association* **95**, 249–262.

Thompson, R. N., Morrison, M. A., Dickin, A. P. & Hendry, G. L. (1983). Continental flood basalt... Arachnids rule OK? In: Hawkesworth, C. J. & Norry, M. J. (eds) *Continental Basalts and Mantle Xenoliths*. Nantwich: Shiva, pp. 158–185.

Wasserburg, G. J., Jacobsen, S. B., DePaolo, D. J., McCulloch, M. T. & Wen, T. (1981). Precise determination of Sm/Nd ratios, Sm and Nd isotopic abundances in standard solutions. *Geochimica et Cosmochimica Acta* **45**, 2311–2323.

Wilcox, C. A. (1954). Petrology of Paricutin Volcano, Mexico. *US Geological Survey, Bulletin* **965-C**, 281–353.

Woodhead, J., Eggins, S. & Gamble, J. (1993). High field strength and transition element systematics in island arc and back-arc basin basalts: evidence for multi-phase melt extraction and a depleted mantle wedge. *Earth and Planetary Science Letters* **114**, 491–504.

Wright, T. L., Mangan, M. & Swanson, D. A. (1989). Chemical data for flows and feeder dikes of the Yakima Basalt subgroup, Columbia River Basalt Group, Washington, Oregon and Idaho, and their bearing on a petrogenetic model. *US Geological Survey, Bulletin* **1821**, 71 pp.

Zartman, R. E. & Haines, S. M. (1988). The plumbotectonic model for Pb isotopic systematics among major terrestrial reservoirs—a case for bi-directional transport. *Geochimica et Cosmochimica Acta* **52**, 1327–1339.

Zhang, M., Zhou, X. H. & Zhang, J. B. (1998). Nature of the lithospheric mantle beneath NE China: evidence from potassic volcanic rocks and mantle xenoliths. In: Flower, M. F. J., Chung, S.-L., Lo, C.-H. & Lee, T.-Y. (eds) *Mantle Dynamics and Plate Interactions in East Asia. American Geophysical Union, Geodynamics Series* **27**, 197–219.

Zhi, X., Song, Y., Frey, F. A., Feng, J. & Zhai, M. (1990). Geochemistry of Hannuoba basalts, eastern China: constraints on the origin of continental alkali and tholeiitic basalt. *Chemical Geology* **88**, 1–33.

Zindler, A. & Hart, S. R. (1986). Chemical geodynamics. *Annual Review of Earth and Planetary Sciences* **14**, 493–571.

Zonenshain, L. P., Kuzmin, M. I. & Natapov, L. M. (1990). *Geology of the USSR: a Plate-Tectonic Synthesis. American Geophysical Union, Geodynamic Series* **21**, 242.